MARINE & FRESHWATER RESEARCH

Primary productivity induced by iron and nitrogen in the Tasman Sea – An overview of the PINTS expedition

Journal:	*Marine and Freshwater Research*
Manuscript ID:	MF13137
Manuscript Type:	Research paper
Date Submitted by the Author:	02-Jun-2013
Complete List of Authors:	Hassler, Christel; University of Geneva, Institute F. A. Forel; CSIRO Wealth from Oceans Research Flagship, CSIRO Marine and Atmospheric Research; University of Techology, Sydney, C3 - Plant Functional Biology and Climate Change Cluster Ridgway, Ken; CSIRO Wealth from Oceans Research Flagship, CSIRO Marine and Atmospheric Research Bowie, Andrew; University of Tasmania, Institute for Marine and Antarctic Studies; University of Tasmania, Antarctic Climate & Ecosystems Co-operative Research Centre Butler, Edward; CSIRO Wealth from Oceans Research Flagship, CSIRO Marine and Atmospheric Research Clementson, Lesley; CSIRO Wealth from Oceans Research Flagship, CSIRO Marine and Atmospheric Research Doblin, Martina; University of Techology, Sydney, C3 - Plant Functional Biology and Climate Change Cluster Davies, Diana; CSIRO Wealth from Oceans Research Flagship, CSIRO Marine and Atmospheric Research Law, Cliff; National Institute of Water and Atmospheric Research (NIWA), Ralph, Peter; University of Techology, Sydney, C3 - Plant Functional Biology and Climate Change Cluster van der Merwe, Pier; University of Tasmania, Antarctic Climate & Ecosystems Co-operative Research Centre Watson, Roslyn; CSIRO Wealth from Oceans Research Flagship, CSIRO Marine and Atmospheric Research Ellwood, Michael; Australian National University, Research School of Earth Sciences
Keyword:	phytoplankton, nutrient dynamics, biodiversity, primary production, oceanography

Primary productivity induced by iron and nitrogen in the Tasman Sea – An overview of the PINTS expedition.

C.S. Hassler[1, 2, 3*]; K. R. Ridgway[2]; A. R. Bowie[4, 5]; E.C.V. Butler[2, #]; L. A. Clementson[2]; M. A. Doblin[1]; D. M. Davies[2]; C. Law[6]; P. J. Ralph[1]; P. van der Merwe[4]; R. Watson[2]; M. J. Ellwood[7]

[1] Plant Functional Biology and Climate Change Cluster, University of Technology Sydney, PO Box 123, Broadway, 2007, NSW, Australia.

[2] CSIRO Wealth from Oceans Research Flagship, and CSIRO Marine and Atmospheric Research, Castray Esplanade, Hobart, 7000, TAS, Australia.

[3] Institute F.-A. Forel, University of Geneva, 10 rte de Suisse, 1290 Versoix, Switzerland.

[4] Antarctic Climate & Ecosystems Co-operative Research Centre, University of Tasmania, Private Bag 80, Hobart, 7001, TAS, Australia.

[5] Institute for Marine and Antarctic Studies, University of Tasmania, Private Bag 129, Hobart, TAS 7001, Australia.

[6] National Institute of Water and Atmospheric Research (NIWA), 301 Evans Bay Parade, Greta Point, PO Box 14-901, Kilbirnie, Wellington, New Zealand.

[7] Research School of Earth Sciences, Building 61, Mills Road, Australian National University, Canberra, ACT 0200.

[*]Corresponding author: Christel.Hassler@unige.ch

[#] present address: Australian Institute of Marine Science, Arafura Timor Research Facility, PO Box 41775, Casuarina NT 0811, Australia.

Abstract:

The Tasman Sea and the adjacent Sub-Antarctic zone (SAZ) are economically important regions, where the parameters controlling the phytoplankton community composition and carbon fixation are not yet fully resolved. Contrasting nutrient distributions as well as phytoplankton biomass, biodiversity and productivity we observed between the North Tasman Sea and the SAZ. In-situ F_V/F_M, dissolved and particulate nutrients, iron biological uptake, and nitrogen and carbon fixation were used to determine the factor limiting phytoplankton growth and productivity in the North Tasman Sea and the SAZ. Highly productive cyanobacteria dominated the North Tasman Sea. High atmospheric nitrogen fixation and low nitrate dissolved concentrations indicated that non-diazotroph phytoplankton are nitrogen limited. Deck-board incubations also suggested that, at depth, iron could limit eukaryotes, but not cyanobacteria in that region. In the SAZ, the phytoplankton community was dominated by a bloom of haptophytes. The low productivity in the SAZ was mainly explained by light limitation, but nitrogen, silicic acid as well as iron were all depleted to the extent that they could become co-limiting. This study illustrates the challenge associated with identification of the limiting nutrient as it varied between phytoplankton groups, depths and sites.

Keywords: nutrients, limitation, subantarctic zone, phytoplankton, bioavailability

Running Head: Nutrient and light limitation in the Tasman Sea

Introduction:

The oceans absorb between 30 and 40% of annually emitted anthropogenic carbon dioxide (CO_2; Battle et al. 2000), representing an important role in Earth's climate system. Photosynthetic micro-organisms responsible for biological carbon fixation are also acting as marine ecosystem engineers, regulating ocean chemistry and driving the biogeochemical cycles of many key elements including, nitrogen, phosphorus, silicic acid, iron, sulfur and carbon (Karl 2000; Chisholm 2000; Morel and Price 2003; LeBlanc et al. 2005; Moore et al. 2009; Boyd and Ellwood 2010). Phytoplankton therefore play a central role in the metabolism of marine systems.

Nutrient limitation imposed by low concentrations of iron (Fe) and nitrogen as nitrate in surface waters affects the growth of phytoplankton in up to 50% of the world's oceans, including low-nutrient, low-chlorophyll (e.g., the North Atlantic and North Tasman Sea; Moore et al. 2009; Law et al. 2011), and high-nutrient, low-chlorophyll regions (e.g., the Southern Ocean; Martin et al. 1990; Boyd and Ellwood 2010), as well as coastal areas (e.g., the California upwelling region; Hutchins and Bruland 1998). The widespread significance of these two nutrients is due to their low concentrations in surface waters, their biological importance and also their biogeochemical "coupling", with Fe being required for atmospheric N_2 fixation and nitrate assimilation (Morel and Price 2003). Indeed, Moore and Doney (2007) have suggested that "iron is the ultimate limiting nutrient leading to nitrogen being the proximate limiting nutrient over wide regions today". Vertical supply of Fe and nitrate in the mixed layer, although not the sole source, can be important to sustain phytoplankton growth (e.g., Bowie et al. 2009; Law et al. 2011). With predictions of shallower mixed layer depths in the future (IPCC 2007), the impact that Fe, N and light availability have on phytoplankton growth and abundance needs to be addressed in the context of present day oceans.

The Tasman Sea and the SAZ are both important regions for Australian biodiversity and socio-economy. The Tasman Sea is a hot spot for climate change with one of the highest predicted oceanic temperature increases due to changes in the strength of major boundary currents (East Australian Current, EAC; Hobday et al. 2008). In addition, contrasting concentrations of nutrients are reported, with macronutrient-(N, P and Si)-poor, warmer subtropical waters in the North (e.g., Ellwood et al. 2013) grading to macronutrient-rich,

colder subantarctic waters in the South (e.g., Bowie et al. 2011). Previous studies also demonstrated a greater dissolved iron concentration in the North Tasman Sea compared to the SAZ (Boyd and Ellwood 2010; Lannuzel et al. 2011; Ellwood et al. 2013). The global ecosystem model developed by Moore and co-workers (Moore and Abbott 2000; Moore et al. 2002) predicts that nutrient distributions and their delivery to the mixed layer of this region would result in contrasting regional phytoplankton nutrient limitation leading to differences in their biomass, biodiversity, primary productivity, and carbon export during the austral summer. Recent studies demonstrated that in the oligotrophic North Tasman Sea, phytoplankton are mainly limited by the lack of nitrogen (Ellwood et al. 2013) with diazotrophs, able to bypass nitrate limitation by fixation of atmospheric N_2, present in surface waters (Law et al. 2011). However, it has been suggested that the growth of diazotrophs in Northern Australia waters and the North Tasman Sea is mostly iron-limited (Kutska et al. 2003; Law et al. 2011). In the SAZ east of Australia, phytoplankton groups are predicted to be mainly limited here by Fe, with Si limitation possible for diatoms (Moore et al. 2002).The region spanning the North Tasman Sea to the SAZ is thus ideal for the study of the influence of iron and nitrogen limitation on phytoplankton communities.

This paper presents selected results from the PINTS ('Primary productivity induced by Iron and Nitrogen in the Tasman Sea') research voyage which took place during the austral summer of 2010. This project identified the distribution of Fe and N and other nutrients from the oligotrophic North Tasman Sea to the highly productive SAZ region in the South Tasman Sea. By comparing the distribution of nutrients with resident phytoplankton communities, and by relating these to key processes at play, such as N_2 fixation, Fe bioavailability, photophysiology and primary productivity, we investigated the control that nutrients and light impose on phytoplankton growth, biodiversity and carbon fixation. This study thus evaluates the distribution of Fe as a key essential trace element, including sink and source processes that affect both its distribution and biogeochemical cycling, and also contributes to the international GEOTRACES program in the Tasman Sea, a region identified as an area of interest for coarse-resolution global surveys of ocean surface waters in the GEOTRACES Science Plan (2006, http://www.geotraces.org/libraries/documents/Science_plan.pdf).

Methods:

Study region

During the PINTS voyage, 18 stations were sampled within the Tasman Sea during the austral summer 2010 (23rd Jan. – 15th Feb. 2010, *RV Southern Surveyor*, Table 1, Fig. 1). The voyage track consisted of three transects, with Transect 1 comprising five stations from Sydney to the oligotrophic North Tasman Sea (P1, 30ºS). It crossed both the narrow abyssal basin (4500-m) off Sydney and the Lord Howe Rise (LHR) which stretches northward through the central Tasman. Transect 2 was a meridional transect from the Northern Tasman Sea (P1) to the SAZ (46.2ºS, P3) recrossing the LHR at 35ºS and extending again into abyssal waters in the south, with eight stations along its length. Transect 3 comprised seven stations extending zonally from the SAZ (P3) to the Tasman shelf (station [Stn] 19) crossing the abyssal plain.

Here, we place the PINTS voyage in the context of the regional circulation. Fig. 2a & b show the general structure of the mean EAC flow off eastern Australia as determined from multi-year ocean measurements (Ridgway et al. 2002). Transect 1 was aligned roughly along the core of the meandering eastward flow of the Tasman Front (TF; Godfrey et al. 1980). It is the portion of the EAC that separates from the western boundary at 31–34°S and extends across the Tasman Sea to the northern tip of New Zealand, forming the East Auckland Current (Fig. 2a, c). The transect also passed through a significant recirculation feature contained within the abyssal waters off Sydney (Fig. 2c). Fig. 2b indicates that from the coast to 160°E the region is very turbulent, dominated by mesoscale eddies, which have a strong signature in surface pressure and thus sea level. These eddies are 200–300 km in diameter and two or three eddies are generated annually and have lifetimes often exceeding a year (Nilsson and Cresswell 1981; Bowen et al. 2005). Fig. 2 shows that Transect 2 traversed the TF and a further series of relatively weak eastward components (Ridgway and Dunn 2003). It also passed through different water masses from subtropical waters north of the TF through to the northern edge of the Subtropical Convergence. The transect was just at the eastern edge of the region of high sea level variability (Fig. 2b), but there was still sufficient mixing to reduce any sharp frontal regions. Finally, Transect 3 encountered mostly quiescent conditions until it reached within 200-km of the Tasmanian east coast, where it met the southern extent of the EAC eddy field and the residual southward component of the EAC (EAC Extension). This latter feature turns both

eastwards southeast of Tasmania towards New Zealand (Bowie et al. 2011) and westward south of Tasmania – the Tasman Outflow – feeding the continental boundary current south of Australia and eventually is incorporated into the southern Indian Ocean gyre (Ridgway and Dunn 2007).

Water sampling

Salinity, temperature, fluorescence and oxygen were obtained from calibrated conductivity-temperature-depth (CTD, SeaBird SBE11) data using water collected from Niskin bottles (General Oceanics) (Reynolds and Navidad 2012). Macronutrients (reactive phosphorus, PO_4; silicic acid, Si; nitrate-plus-nitrite, NO_x) were obtained by the shipboard analysis of unfiltered water using an automated flow-injection analyser and colorimetric techniques (Reynolds and Navidad 2012). Analytical detection limits were 0.011, 0.013 and 0.016 μM for NO_x, PO_4 and Si, respectively (A. Navidad, pers. comm.). Samples were also collected from the CTD rosette for the determination of pigments concentration and composition, photophysiology, primary productivity, and N_2 fixation rate.

Since Fe and most of the other micronutrient elements are trace metals omnipresent in shipboard environments, samples for almost all the procedures below required the use of accepted and verified non-contaminating sampling procedures. In this case water was sampled directly after the deployment of the CTD (within 30–60 min of CTD recovery) using Teflon-coated Niskin X-1010 bottles (General Oceanics, USA) mounted on an autonomous rosette (Model 1018, General Oceanics, USA) and deployed using a Dynex hydroline (*Dynex Dyneema* 75, Hampidjan, Ltd, Nelson, New Zealand). Water samples for trace micronutrient analysis were collected and filtered (Pall, Acropack 200) in a clean van under a HEPA filter (ISO Class 5 conditions). Unfiltered seawater was also sampled for macronutrient analysis, and the determination of the iron biological uptake rate by the natural phytoplankton community. Sample acquisition and handling was as per GEOTRACES recommendations (Cutter et al. 2010; www.geotraces.org/libraries/documents/Intercalibration/Cookbook.pdf), using acid-washed non-contaminating material as detailed elsewhere (O'Sullivan et al. 1995; Bowie et al. 2009; Lannuzel et al. 2011). Samples were acidified using quartz-distilled HCl (qHCl, Seastar Baseline, Canada) to 0.02 M qHCl and kept for six months double-bagged in plastic boxes in clean storage, prior to analysis.

Synthetic Temperature-Salinity - synTS

To provide further regional context for the cruise sections, we obtained temperature and salinity fields generated from surface height (altimetry) and SST from satellite data (synTS; Ridgway et al. 2008). The system uses a multiple linear regression model obtained from historical in-situ observations.

Dissolved metal analysis

Dissolved iron (dFe) was determined by flow injection analysis with chemiluminescence detection (FI-CL) using in-line preconcentration on a TOYOpearl-8HQ chelating resin column adapted from Obata et al. (1993) and de Jong et al. (1998). Accuracy was checked using an in-house quality control (QC) standard and by analysing the surface standard (S1) collected during the SAFe cruise (Johnson et al. 2007) (S1 = 0.109 ± 0.007 nM compared to the 'certified' value of 0.097 ± 0.043 nM). The mean limit of detection (LOD) was 0.04 ± 0.04 (n=21) for a 3 minute load. An automated method of flow injection – solid-phase extraction – inductively coupled plasma-mass spectrometry (FI–SPE–ICPMS) was used for determining dissolved Cd as detailed in O'Sullivan et al. (2013). Detection limit and precision of Cd analysis was of 5 pM and 3 %, respectively. Accuracy was checked using certified standard (SAFe D2) and reference seawater (NASS-5, National Research Council of Canada). Value of 904 ± 41 (n=11) and 190 ± 11 (n=11) pM of Cd were obtained for SAFe D2 and NASS-5, respectively. Values were within the certified range 1011 ± 28 pM and 205 ± 30 pM for SAFe D2 (http://es.ucsc.edu/~kbruland/GeotracesSaFe/kwbGeotracesSaFe.html, Nov. 2011) and NASS-5, respectively.

Particulate metal analysis

Suspended particulate trace metal samples were collected in situ using a 142 mm diameter stack consisting of a 54 µm polyester pre-filter screen (Sefar Filtration, Inc.) followed by a Whatman QMA filter (nominal pore size 1 µm), following methods outlined in Bowie et al. (2009). Filter stacks were housed in large volume McLane pumps (McLane Research Laboratories Inc., USA) suspended on plastic-sheathed steel mooring wire. Filters and supports were prepared and pre-cleaned as described in Bishop et al. (1985). Upon recovery of the pumps, filters were dried under a laminar flow bench and sub-samples taken using a circular plastic punch (15 mm diameter). Filters were stored frozen at -20 ºC in acid-washed petri dishes until further analysis in the home laboratory. Blanks were true

'field' blanks that were deployed in situ (i.e., filter stacks that no seawater had passed through on the McLane pumps).

Sampled particles were acid extracted (1 mL concentrated HNO_3 for 12 h at 95 ºC) in Teflon PFA vials and analysed by magnetic sector inductively coupled plasma mass spectrometry (Finnigan ELEMENT 2) offering high spectral resolution capability, following methods reported in Cullen and Sherrell (1999), Townsend (2000), and Bowie et al. (2010). Recoveries for Fe were verified by analysing a certified reference material for marine and plankton (Community Bureau of Reference BCR-414, with a mean recovery of 89% % for Fe (n=3) using HNO_3 only as the digestion solution.

POC/ PON analysis

Water collected from the CTD was filtered through muffled quartz 1µm filters (450 °C for five hours, Sartorius). The filters were then de-carbonated by fuming overnight in hydrochloric acid and then drying for 48 h at 60 ^{0}C in a clean oven, to drive off excess acid and ensure dryness. The active area of the filter (22.5 mm dia.) was subsampled, in a class 1 laminar flow cabinet (Gelman CF43S), with a single 18 mm punch. The filter punching was then encapsulated in silver 9 × 5mm capsules (Sercon SC0037) as preparation for elemental analysis. Unused muffled filters were processed similarly to use as an analytical blank. The capsules were stored over silica gel prior to analysis. McLane filter subsamples (13.8 mm subsample of 133 mm active area) were transferred directly to capsules and de-carbonated by acidification with two 20 µL aliquots of 2 M HCl (King et al. 1998), followed by drying for 48 h before crimping and compressing the capsules. Certified casein (OAS Elemental Microanalysis) was included with the samples as a further analytical quality control.

The POC/ PON analysis was performed using a gas chromatography elemental analyser (Thermal Finnigan Flash 1112 series catalytic combustion) run in standard conditions with reference to acetanilide standards in the Central Sciences Laboratory of the University of Tasmania. Precision of the analyses was 1% (Dr. Thomas Rodemann, pers. comm.).

Phytoplankton pigments

Pigment samples were collected on GF/F filters (Whatman) using gentle filtration (< 5 mm Hg) and stored in cryo-vials in liquid nitrogen prior to being analysed back on shore. The

pigments were extracted in 100% methanol in the dark and at 4 °C and analysed by HPLC using a Waters – Alliance high performance liquid chromatography system, comprising a 2695XE separations module with column heater and refrigerated autosampler and a 2996 photo-diode array detector following a modified version of the Van Heukelem and Thomas (2001) method (see Hassler et al. 2012a for details). Concentrations of chlorophyll-*a* (Chl-*a*), chlorophyll-*b* (Chl-*b*) and β,β-carotene in sample chromatograms were determined from standards from Sigma, while all other pigment concentrations were determined from standards from DHI (Denmark). The presence or absence of pigments which relate specifically to an algal class, termed biomarkers, was used to provide a simple guide to the composition of a microalgal community, including identifying classes of small flagellates that could not be determined by light microscopy techniques (Jeffrey and Wright, 2006). Biomarker pigments analysed were Fucoxanthin (Fuco), 19-Butanoyloxyfucoxanthin (But-Fuco), 19 Hexanoyloxyfucoxanthin (Hex-Fuco), Zeaxanthin (Zea), Chlorophyll *b* (Chl-*b*), Peridinin (Peri) and Divinyl Chlorophyll-*a* (DVChl-*a*).

Flow cytometric enumeration of picoplankton

Samples for enumeration of bacteria and cyanobacteria were fixed with 1% (v/v final concentration) glutaraldehyde, frozen in liquid nitrogen and stored at -80 °C. Bacterial enumeration was performed on samples stained with SYBR Green I (1:10,000) (Invitrogen) (Marie et al. 1997), while cyanobacterial analysis was performed using unstained samples. Samples were analysed using a Becton Dickinson LSR II flow cytometer. Bacterial populations were discriminated according to SYBR Green fluorescence and side-scatter (SSC) (Marie et al. 1997), while populations of *Prochlorococcus* and *Synechococcus* were discriminated using SSC and red and orange fluorescence. Data was analysed using Cell-Quest Pro (BD Biosciences) as in Seymour et al. (2012).

Photophysiological community analysis

To assess the photosynthetic efficiency (F_V/F_M) of phytoplankton community in-situ, a prototype submersible Pulse Amplitude Modulated Water PAM (sub-Water PAM, Gademan Instruments GmbH, Würzburg, Germany) fluorometer was deployed with the CTD to a maximum depth of 100 m. The instrument had two channels (red and blue LED, with wavelengths of 620 and 480 nm, respectively) to collect data on the photosynthetic activity of the total phototrophic community and the total minus cyanobacteria community,

respectively. The sub-Water PAM was programmed to pump water for 10 s to flush the dark chamber every 5 min. Profiles were conducted by lowering the instrument at 10 m intervals and maintaining position for 10 min. At each depth, a saturating pulse of light (pulse duration = 0.6 s; pulse intensity > 3000 µmol photons m^{-2} s^{-1}) illuminated the sample and maximum fluorescence (F_M) was determined. Maximum quantum yield of photosystem II (PSII), F_V/F_M, was then calculated according to the equation $(F_M-F_0)/F_M$ (Schreiber 2004).

^{14}C productivity

Radiolabeled sodium bicarbonate ($NaH^{14}CO_3$, Perkin Elmer) was added to freshly sampled surface and subsurface chlorophyll-a maximum seawater to produce a working solution of 39.183 x 10^3 Bq per mL (1.1 µC mL^{-1}). Primary productivity incubations were conducted as described in Doblin et al. (2011), based on the small bottle ^{14}C technique of Lewis and Smith (1983). Briefly, a working solution was initially sampled to determine initial radioactivity, then triplicate 7 mL aliquots were each incubated in glass vials for 1 hour in the dark and at 2 light intensities at in-situ temperature (± 0.5°C) controlled using a water-bath, or for surface seawater, using running seawater pumped from a depth of 5 m. Inorganic carbon was degased by the addition of 250 µL of 6 M HCl (Technical grade, Crown Scientific) and agitated for 3 h prior to addition of 10 mL scintillation cocktail (Aquasure, Perkin Elmer) and counting using a TriCarb 2900 scintillation counter (Packard, Waltham MA, USA). Counts per minute were transformed into disintegration per minute using the built-in quench curve and radioactivity was expressed in carbon fixed per volume per hour using initial radioactivity and dissolved inorganic carbon (DIC) analysed using coulometric procedures (Johnson et al. 1998). Carbon uptake rates were standardised with in-situ Chl-*a* concentrations measured using HPLC.

Iron bioavailability

Phytoplankton iron uptake rates (amol Fe µg Chl-a^{-1}) were used to estimate iron bioavailability as per Hassler and Schoemann (2009a). One litre of unfiltered seawater, freshly collected from the depth of maximal fluorescence, was spiked with 2 nM $^{55}FeCl_3$ (Perkin Elmer, 20.82 mCi/mg Fe at the time of use). Solutions were sub-sampled (2 mL) to measure total initial radioactivity, then incubated for 20-24 h at in-situ temperature and light as determined from CTD deployments. Following incubation, the phytoplankton was gently sequentially filtered (< 5 mm Hg, 10 µm polycarbonate filter [Millipore], then 2 µm

and 0.7 µm glass fiber filters [MicroAnalytix]) and rinsed (5 × 3 mL, total contact time 10 min.) with an EDTA-oxalate solution to discard the adsorbed iron (Hassler and Schoemann 2009b). The filter was then rinsed with filtered seawater (3 × 3mL, < 0.7 µm), collected in scintillation vials, supplemented with 10 mL of scintillation cocktail (Ultima Gold, Perkin Elmer) and then analysed using a liquid scintillation counter (Perkin Elmer, Tricarb 2900). Intracellular disintegrations per minute were transformed into iron concentration using a custom made quench curve, total initial radioactivity and dissolved iron concentration (see Hassler and Schoemann 2009a for details). Pigment analyses were performed (see above) in order to normalise iron uptake rate by phytoplankton biomass and investigate differences in the iron uptake rate for the different dominant taxa in the micro- (> 10 µm), nano- (2-10 µm), and pico-plankton (0.7-2 µm). Incubations were done in duplicate.

Nitrogen fixation

2.4-Litres were sub-sampled from the Niskin bottles into acid pre-washed polycarbonate bottles (Nalgene). 4.5 mL of 99% ^{15}N-N_2 was then injected through a butyl rubber septum in the lid, followed by gentle rotation to encourage dissolution and subsequent incubation for 24 hours in on-deck incubators (as per Law et al. 2011). The incubations were terminated after 24 hours by filtration under low negative pressure onto pre-ashed 25 mm 0.7 μm Whatman GF/F filters, which were stored in a -20 ^{o}C freezer. Background ^{15}N-PON natural abundance was determined by filtration of 2.4 L surface seawater that was not spiked with ^{15}N-N_2. All filters were subsequently dried and analysed for ^{15}N incorporation into PON by stable isotope mass spectrometry using an NA1500 elemental analyser (Fisons Instruments) interfaced to a Delta^{plus} (Thermo-Finnigan) continuous flow isotope ratio mass spectrometer (CF-IRMS), with nitrogen fixation rates determined using the calculations of Montoya et al. (1996). The calculations were based on a dissolved concentration of 1.14 +/-0.09 mL/L, as reported in Law et al. (2011), following identification that dissolution of ^{15}N-N_2 was not instantaneous (Mohr et al. 2010).

Results:

Oceanography – Syn TS

The temperature along the PINTS track obtained from SynTS is compared with the observed data from the CTD stations in Fig. 3. The section shows the temperature

anomaly (the mean field from a climatology (CARS; Ridgway et al. 2002) has been removed). The SynTS result is in good agreement along the Transect 1, capturing the main structure at the right magnitude. Along Transects 2 and 3, the comparison is not quite as good. While the inferred SynTS temperature does show a similar pattern of warm and cool anomalies along the track the magnitude of the features is far smaller. For example, there was a strong negative feature (< -4 °C) in the upper 125 m at cast 8 in the observed section, which is only weakly negative in the SynTS result. However, despite the smaller amplitude of the SynTS features these comparisons suggest that the SynTS fields will provide a very useful summary of the circulation at the time of the voyage.

The SynTS fields of *T* and *S* in Fig. 4 show the main features in the region during the cruise. We see that the cruise track passed through the highly energetic EAC eddy field. Steaming out of Sydney the track crossed a large cold-core cyclonic eddy and then passed between the separated EAC flow (wrapped around an anti-cyclonic feature) to the north and another warm-core anti-cyclonic eddy that had almost completed 'pinching off' from the main EAC structure. The track then passed through the centre of another anti-cyclonic eddy (158°E) although the nearest station (Stn 3) was located on the edge of the eddy. The eastern transect passed through a train of less energetic anti-cyclonic and cyclonic features from 30 to 38°S, although the stations tended to be on the periphery of the eddies. Moving southwards, the transect passed from a higher to lower salinity environment with a distinct salinity front from 43-45°S (Fig. 4). Even at 1000 m where salinity gradients were small there was a frontal region representing the boundary between Antarctic Intermediate Water (AAIW) of southern origin and the higher salinity northern variant which has been modified as it is advected around the South Pacific Gyre (Sokolov and Rintoul 2000). On the southern transect, the voyage moved into the SAZ and the track passed through a region of meandering filaments from the north and south. Finally as it approached eastern Tasmania it again crossed the EAC sourced waters associated with a seasonal warm-core eddy at 148°E (Ridgway 2007).

Oceanography – Temperature, Salinity, Oxygen

The salinity, temperature and oxygen from the CTD stations occupied along the PINTS voyage track are presented in Fig. 5. In the following presentation of the voyage results we recognize that the sampling interval of the CTDs was not able to completely resolve the highly energetic EAC eddy field. However, the sections did clearly show that the track

sampled two distinct oceanic regions – a warm, salty, low oxygen water mass associated with the EAC that enters the Tasman Sea from the north and east of the South Pacific Gyre (Sokolov and Rintoul 2000) and a cool, fresh, high oxygen water mass that is sourced from the subantarctic region in the south. The transition between these two regions occurred fairly sharply at 44°S which represents the Sub-Tropical Front (STF). This tends to extend slightly northward between Tasmania and New Zealand (Orsi et al. 1995; Ridgway and Dunn 2007). The *T* and *S* sections also indicated that the track crossed another frontal zone between 32 and 35°S, the Tasman Front, which represents the separated EAC flow meandering eastward across the Tasman Sea (Figs. 4c-d; Godfrey et al. 1980). An anomaly section of *T* (not shown) indicated that the summer mixed layer penetrates to 20–30 m in the north and east and from 50–60 m along the southern transect (Transect 3).

The cold-core eddy off Sydney at the start of the track had a distinct subsurface expression, with low *T* and *S* from 60–900 m and also a smaller cell of low oxygen from 50–150 m. Station 3 showed the typical eddy induced deepening of the thermocline despite it being located to the west of the eddy centre. There was no corresponding salinity signature, because the salinity was well mixed down to about 150 m north of the Tasman Front (Fig. 4). In fact, Fig. 5 showed a uniform high salinity feature in this region with the maximum in salinity occurring in the northeastern corner of the cruise track (Stns 4–6). The Tasman Front was shown by a subsurface frontal region in both *T* and *S* between 50-250 m (Fig. 5). There was also a strong expression in both *T* and *S* at the STF in the upper 400 m (44°S) which extended down to about 400 m. Along the southern Transect 3 both *T* and *S* showed an alternating series of high and low features extending to 400 m. They features identified the cross-frontal exchange of properties, northward intrusions of cool, fresh, subantarctic water and warm, salty water from the north. East of Tasmania, at the end of the voyage track, the high *T* and *S* associated with the anti-cyclonic eddy projected down to more than 1000 m.

The dissolved oxygen section (DO, Fig. 5c) showed a high degree of structure along the path. The magnitude and vertical extent of DO increased uniformly – the depth of the 220 µM contour increased from 50 m east of Sydney to 800 m southeast of Tasmania. In fact the advection of high DO water into the southern Tasman Sea was associated with cross-frontal processes indicated by the Subantarctic intrusions at 152°E (Figure 5). The DO signature of these intrusions extended deeper than that of *T* and *S* (> 800 m). A thin

filament (40 m) of high DO water at 60 m depth was sampled along the section from 43°S to the Sydney endpoint. It was apparently formed in the south Tasman (at the surface) and spreads northwestwards along the 25.4 isopycnal.

Macronutrients

Although the distance between CTD deployments was too great to efficiently resolve the oceanography in Transect 1 and 2 (see above), the effect of mesoscale features can be seen on macronutrient distributions, with doming of isolines along Transect 1 (Fig. 6 and Suppl. Fig. 2). In general, for a given depth along Transect 1, the concentrations of NO_x, PO_4 and Si decreased eastwards (P1, Stn 5). At P1, the surface water was strongly depleted in macronutrients (NO_x < 0.011 µM, PO_4 0.02–0.12 µM, Si < 0.7–1.0 µM). Indeed concentrations of NO_x using a nanomolar analytical method were on average 8.5, 9.2, and 9.8 nM at 15, 30 and 50 m depth respectively (M. Woodward, pers. comm.). Along Transect 2, macronutrient concentrations generally increased from North (P1) to South (P3, Fig. 6, Suppl. Fig. 2). A doming of all macronutrients in surface water north and in the STF was observed from Stn 7 to 11 with depleted concentrations at P3 (Suppl. Fig. 2). As previously observed (Ellwood et al., 2013), despite crossing the Tasman Front, no frontal footprint in macronutrient concentrations was observed (down to 1000 m depth). Along transect 3, macronutrient concentrations increased towards Tasmania, but remained lower at depth (1000 m) than measured along Transects 1 and 2 (Fig. 6). As for Transect 1, mesoscale features affected macronutrient distribution, resulting in doming isoclines. Close to Tasmania (Stns. 17 and 18), surface water was depleted in NO_x and PO_4, but not Si, possibly resulting in a heterogeneous diatom distribution along Transect 3 (Suppl. Fig. 2). Considering all data, the dissolved NO_x :PO_4 disappearance ratio was 14.7 ±0.1 (r^2 = 0.98, *n*= 386).

Organic particles

Total Chl-*a* concentration was used as a surrogate of phytoplankton biomass. Patchiness of Chl-*a* was measured along all transects (Fig. 7a). Overall, the total Chl-*a* in surface water (0–125 m) was well correlated with the fluorescence data from CTD deployments (Suppl. Fig. 3) and increased along the cruise track, with maximum values observed in the SAZ region (P3 and Stn 14). Along Transect 1, the depth of the maximum Chl-*a* decreased from 40 m to 110 m with very low Chl-*a* concentrations for the top 50 m (0.2 µg L^{-1} isocline) at

P1. Close to the LHR (Stn 3), two distinct Chl-*a* maxima were measured. Travelling southwards from P1 to P3, the total Chl-*a* in surface water increased with a shallower depth of Chl-*a* maximum. At P3, the maximum Chl-*a* was found in surface waters (top 25 m). Moving west along Transect 3, the total Chl-*a* in surface water decreased toward Tasmania and the Chl-*a* maximum deepened from 25 m (P3) to 40–50 m (Stn 18).

POC and PON were measured in surface water (25 m) and at the depth of the maximal fluorescence (Suppl. Fig. 3) along the cruise track. As expected, the ratio Chl-*a*: POC and Chl-*a*: PON was statistically lower ($p<0.001$) in surface waters (0.30 ± 0.09; 0.03 ± 0.01 μg μmol^{-1}, n = 17, respectively) than at the depth of maximum fluorescence (0.73 ± 0.41; 0.10 ± 0.04 μg μmol^{-1} n = 18, respectively). At the depth of maximum fluorescence, the Chl-*a*: POC ratio was greater (> 0.65 μg μmol^{-1}) at Stns 2, 5–8, 9-10 and 16–18, coinciding with high Chl-*a*: PON (> 0.09 μg μmol^{-1}). Particulate material at the surface showed a different pattern (data not shown). The greatest ratios for Chl-*a*: POC and Chl-*a*: PON at the depth of fluorescence maximum were observed at Stn 5 (1.99 μg μmol^{-1}), and Stns 2, 16 and 18 (0.12 μg μmol^{-1}), respectively. The lowest ratios for Chl-*a*: POC and Chl-*a*: PON at the depth of fluorescence maximum were observed at Stns 4 and 13 (0.37–0.38 μg μmol^{-1}) and Stn 4 (0.04 μg μmol^{-1}).

The POC: PON ratio (or C/N, Fig. 7b) was used to indicate a potential nitrogen (N) limitation. A ratio of C/N above the optimal Redfield ratio (6.6; Redfield et al. 1963) indicates a deficit of nitrogen relative to carbon in organic matter, possibly related to N limitation. In the study region, the ratios C/N were in general greater in surface water. The C/N ratios were close to the Redfield ratio from Stns 12 to 15 in surface water (25 m), and at Stn 4 and Stns 10 to 17 at the depth of maximal fluorescence. An extremely high value (16.5) was measured in surface waters at Stn 7. C/N was weakly correlated to Chl-*a* (r^2 = 0.42, n= 29) for C/N value < 10.0 (4 points were excluded, all of which had Chl-*a* < 0.2 μg/L). The negative slope (-0.19 ± 0.04), suggests that greater phytoplankton growth were observed at lower C/N ratio.

Comparison between North Tasman Sea (P1) and SAZ (P3)

Overall for the study region, the greatest differences in fluorescence (and Chl-*a*), macronutrient profiles, as well as C/N were observed in Transect 2 between P1, the North

Tasman Sea, and P3, the Sub-Antarctic Zone. Below, we present more detailed results to investigate differences in phytoplankton abundance, biodiversity and productivity in relation to both macro- and micro-nutrients at these two sites.

Nutrient distribution- The concentrations of the macro- (NO_x, PO_4, Si) and micro-nutrient Cd were greater in surface water and at the depth of maximum fluorescence for P3 compared to P1 (Fig. 8, and Suppl. Fig 4). Only for Fe, the concentrations in surface waters and at depths of maximum fluorescence were smaller at P3. For depths greater than 2000 m, nutrient concentrations were greater at P1, suggesting differences in the source, sink and transport of nutrients for these two sites.

The Fe* was calculated to discuss potential dFe limitation for phytoplankton growth. The Fe* at a given site and depth compares the concentrations of dFe and PO_4 concentrations with respect to Fe and P phytoplankton cellular quota ($R_{Fe:P}$). Fe* equals [dFe]-$R_{Fe:P}$ x [PO_4], and an average phytoplankton $R_{Fe:P}$ was considered (0.47 mmol: mol; Parekh et al. 2005). A negative Fe* is indicative of Fe limitation (Parekh et al. 2005; Bowie et al. 2009; Lannuzel et al. 2011). Here, Fe* decreased with depth from 0.29 at 15 m to -0.01 at 95 m for P1 and from 0.09 at 15 m to -0.06 at 80 m at P3. Negative Fe* values for the top 100 m were only observed at 95 m and 80 m at P1 and P3, respectively.

The disappearance ratios Cd: PO_4, PO_4: NO_x, Fe: PO_4 were similar considering all data from both sites (Fig. 9a – c). A "kink" was observed in the Cd: PO_4 relationship for dissolved concentrations of PO_4 < 0.8 μM, comprising data from 0–125 m at P1 and P3. Fe: NO_x and Fe: Si showed a typical "scavenging" relationship for Fe (Fig. 9e and 9g). When considering only data from 0–125 m, the euphotic zone inhabited by phytoplankton, differences in disappearance ratios for Fe: PO_4, Fe: Si and Fe: NO_x were observed between stations (Fig. 9 d, f, and h, respectively). Dissolved Fe: PO_4 and Fe: Si ratios were greater at P1, suggesting a lower relative biological demand for Fe at this site, possibly related to a limitation Fe utilisation by the low concentrations of PO_4 or NO_x. Using the NO_x concentrations measured at P1 (M. Woodward, pers. comm., 15-50 m) Fe: NO_x ratio was negative (-122 nmol: μmol, $r^2 = 0.98$, n=3).

Phytoplankton biology – The vertical distribution of phytoplankton biomass (Fig. 10d), the cyanobacteria and nanoplankton distribution profiles (Fig. 10b, f) and the dominant phytoplankton groups inferred from biomarker pigments (Fig. 10c, g) were different at P1 and P3. Despite similar total biomass inferred by total Chl *a*, the vertical distribution of phytoplankton is quite different (Fig. 10d). At P1, a deep Chl *a* maximum was observed (90-110 m), whereas high biomass was present in the top 30 m at P3, suggesting difference in nutrients and light availability amongst sites. Order of magnitude greater N_2 fixation rate were measured at P1 relative to P3 (Fig. 10h); as expected from the warmer temperature and the oligotrophic status of P1 (Law et al. 2011). However P1 has an unusual surface mixed layer profile with a maximum N_2 fixation rate at 50m. At P1, cyanobacteria of the type *Prochlorococcus* and *Synechococcus* were present with *Prochlorococcus* dominating at depth of maximal fluorescence, whereas *Synechococcus* dominated at P3 (Fig. 10b and DV Chl-*a* from Fig. 10c). Biomarker pigments demonstrated that haptophytes (Hex-Fucoxanthin) were also present at P1 and diatoms (Fucoxanthin) were only marginally abundant. At P3, cyanobacteria contribution to biomass was less important, and haptophytes were dominating the phytoplankton biomass as suggested by the MODIS calcite map of the study region during the time at sea and coccolithophorids abundances (Mark Baird and Cliff Law, pers. comm.). At P3, diatoms (Fucoxanthin) were more abundant than at P1 and dinoflagellates (Peridinin) were also present (Fig. 10g). This contrast in phytoplankton communities could result in differences in vertical patterns of nutrient and light limitation, primary productivity, generation of detritus and export.

F_V/F_M is commonly used as an indicator for nutrient or light limitation (e.g., Behrenfeld et al. 2006). Here, we measured the in-situ F_V/F_M for the entire phytoplankton community including cyanobacteria (Red excitation) in contrast to the phytoplankton community excluding *Synechoccocus* (Blue excitation; Fig. 10a and e). At P1, the F_V/F_M for both the cyanobacteria and the overall community was lower in surface and increased with depth to reach a maximum value at the depth of maximal fluorescence (95 m). This suggests that light was not limiting at that depth, but nutrient limitation or photo-inhibition processes occurred at shallower depths. Similar F_V/F_M profiles were measured at P3; however, the total phototrophic community showed a more constant and an overall greater F_V/F_M (Red) compared to P1. Sub-optimal F_V/F_M (< 0.6) at the maximum fluorescence P3 suggested that phytoplankton growth was limited. The greater difference in red and blue F_V/F_M at P1

indicated a greater contribution of *Synechococcus* to the total phototrophic signal. The dominance of coccolithophorids at P3 provided a strong haptophyte signal that masked any minor fluorescence signature from the cyanobacteria; this is why both red and blue F_V/F_M values were similar.

As for the dFe concentrations, the particulate iron (pFe) concentrations were lower at the depth of maximal fluorescence at P1 (Table 2). The ratios pFe: POC were similar in surface water at P1 and P3, and lower at depth for P1. In contrast, the ratio pFe: Chl-*a* increased at depth at P1, and was greatest at P3. The dFe concentrations normalised by POC were smaller than the pFe concentrations normalised by POC for both sites, whereas the dFe concentrations normalised by Chl-*a* were greater than pFe: Chl-*a* at site P1 and lower at P3.

The phytoplankton iron uptake rate (Fig. 11a) is a measure of their ability to take up Fe which can be related to Fe biological requirement and Fe limitation (Hassler et al. 2012b). Here, Fe uptake rates were measured for three phytoplankton size classes to elucidate whether Fe differentially controls phytoplankton within the natural community present at the depth of maximal fluorescence. To account for the differences in phytoplankton biomass between sites and size class (Tot Chl-*a*, Fig. 11b), Fe uptake rate was normalised to Chl-*a* (Fig. 11c). At P1, the phytoplankton community composition was dominated by pico- and nano-plankton. From the composition of biomarker pigments (Fig. 11d), the picoplankton were mainly cyanobacteria of the type *Prochlorococcus*, whereas the nanoplankton were mainly haptophytes. The Fe uptake rate per unit of biomass was lower for the picoplankton than for the nanoplankton, suggesting different abilities to take up iron or different iron requirement between prokaryotic and eukaryotic phytoplankton at this site. At P3, iron uptake rates per unit of biomass were similar for pico- and nano-plankton despite greater relative abundance of nano-plankton, suggesting that parameters other than Fe controlled the abundance of phytoplankton at this site. At P3, the size classes did not resolve the different phytoplankton functional groups well with haptophytes dominating and diatoms present in the micro- and nano-plankton size class. Dinoflagellates and cyanobacteria of the *Synechoccocus* type were mainly present in the micro- and pico-plankton, respectively.

Despite a lower F_V/F_M (Red) and biomass of the total phototrophic community in surface water at the site P1 compared to P3, Chl-*a*-specific carbon fixation from the phytoplankton community was greater at P1 (Fig. 12b). It is to be noted that the F_V/F_M (Blue) was greater at P1 relative to P3. The small difference between the biological carbon fixation at low and high light in surface waters, suggest that these communities were well adapted to their in-situ light levels (382 and 56 µmol photons m^{-2} s^{-1} at P1 and P3, respectively). At the depth of maximum fluorescence, the biological carbon fixation was greater at P1 than P3 (Fig. 12c-d). The largest difference in biological carbon fixation between these two sites was observed at low light, suggesting that the phytoplankton community of P1 is well adapted to low light prevailing at depth. At P1, an in-situ light intensity of 25 µmol photons m^{-2} s^{-1} was measured at the depth of 74 m (Suppl. Fig. 3). The large difference in carbon fixation between the low and high light treatment at the site P3 demonstrated that the in-situ biological carbon fixation was not optimal, and limited by the low light intensity found at the depth of maximal fluorescence (13 µmol photons m^{-2} s^{-1} at 25 m).

Discussion:

During the time of the cruise, the oceanography in the region was representative for austral summer (Ridgway and Dunn 2003). A comparison of the PINTS sections with climatological fields did not show any large-scale offsets in temperature, salinity or any other properties; rather the differences were at relatively small spatial scales and likely to be associated with the presence of meso-scale eddies. Despite CTD deployments being too widely spaced to accurately represent the detailed oceanography in the study region, distinctive patterns in the distribution of micro- and macro-nutrients, and total Chl-*a* were observed. Marked differences in most of the parameters studied were observed between the North Tasman Sea and the SAZ southeast of Australia, as also predicted by the model from Moore and co-workers (Moore and Abbott 2000; Moore et al. 2002) and from recent studies (Bowie et al. 2009; Law et al. 2011; Ellwood et al. 2013). Despite observed concentrations for dFe and Chl-*a* being greater than predicted by the mixed-layer ecosystem model (Moore et al. 2002), comparative trends between P1 and P3 were accurate for dFe, Chl-*a*, NO_x, atmospheric N_2 and C biological fixation. As predicted by their model, the greater primary productivity at P1 is not associated with greater carbon export as the phytoplankton community was dominated by small cyanobacteria. The model predicted greater $CaCO_3$ export at P3, which was corroborated by the dominance of

haptophytes, including *Emiliania huxleyii* and the MODIS calcite composite map (this study; C. Law and M. Baird, pers. comm.).

The in-situ F_V/F_M values at P1 and P3 also suggested a growth limitation or a photo-inhibition which significantly differs for the cyanobacteria and the whole phytoplankton community at P1. Despite a sub-optimal F_V/F_M being a good indicator for Fe limitation in high-nutrient-low-chlorophyll regions, previous studies have also reported high F_V/F_M under N and Fe co-limitation (Behrenfeld and Miligan 2013), preventing the use F_V/F_M as a sole indicator of nutrient limitation in our study region.

A 'kink' in the disappearance ratio trend for Cd was observed for the surface waters of P1 and P3, suggesting a decrease in phytoplankton growth rate (Sunda and Huntsman 2000; Cullen et al. 2003). Previous studies in the south Tasman Sea have observed such a trend for $PO_4 < 0.6$ µM, with a similar disappearance ratio at greater PO_4 concentrations (323 and 460 for austral summer and winter, respectively, at 15–100m; Ellwood 2008a; Butler et al. 2012; Hassler et al. 2012a). The parameters usually discussed as a control of phytoplankton growth rate, with an effect on disappearance ratios are: (i) iron limitation (e.g., Martin et al. 1990; deBaar et al. 1997; Cullen et al. 2003), (ii) combined effect of micronutrients (Sunda and Hunstman 2000; Twining et al. 2004; Cullen and Sherrell 2005; Gault-Ringold et al. 2012), and (iii) community structure and differing nutrient requirement (e.g., deBaar et al. 1997; Arrigo et al. 1999; Sunda and Huntsman 2000; Ho et al. 2003; Quigg et al. 2003; Twining et al. 2004; Finkel et al. 2007). In surface waters, a greater disappearance ratio is often associated with a variation in the relative biological uptake but could also be related to different recycling and remineralisation rates. Unfortunately, neither the bacterial loop nor the grazing rates were measured in this study. Owing to previously high grazing rates and remineralisation processes reported in the region (Pearce et al. 2011; Jacquet et al. 2011), further studies should address their impact on disappearance ratio and the biogeochemical cycle of nutrients. Biological requirement can also be modulated by the bioavailability of other nutrients, light, temperature and change of pCO_2 that occur under bloom situations, with impact on disappearance ratios (see Finkel et al. 2010 for a review).

Comparison of the carbon fixation measured under 250 µmol photons m^{-2} s^{-1} with the optimal carbon fixation predicted from in-situ temperature (Behrenfeld and Falkowski

1997; Fig. 12d) suggests that maximal biological carbon fixation was only measured in surface water at P1. It is noted that this maximal carbon fixation at that site was remarkable given the low dissolved NO_x and PO_4 concentrations; the ability to fix atmospheric N_2 is likely essential for an efficient carbon fixation (Ellwood et al. 2013). Sub-optimal carbon fixation has important impacts for carbon export and climate, and could be due to saturating light greater than the 250 μmol photons m^{-2} s^{-1} used in this study (e.g., Westwood et al. 2011) or due to light or nutrient limitation.

Within the study region, nitrogen and iron were the two nutrients that most likely limited phytoplankton growth. Overall the good correlation between C/N to Chl-*a* observed here, suggests that N is a key nutrient for most of the study region, as recently demonstrated in the North Tasman Sea (Ellwood et al. 2013). Despite this, C/N ratios for eukaroytic phytoplankton can significantly differ from the Redfield ratio (6–11; Quigg et al. 2003), with C/N ratios reported for *Trichodesmium* and marine *Synechococcus* and *Prochlorococus* being close to the Redfield ratio (5–6.2; Bertilsson et al. 2003; Kutska et al. 2003; Nuester et al. 2012). At P1, several parameters indicate that nitrogen limitation was an important control of the phytoplankton community in the surface water of P1: these are low NO_x concentrations (< 0.011 μM), a C/N ratio greater than the Redfield ratio (6.6; Redfield et al. 1963), and the presence of diazotrophs fixing atmospheric nitrogen. As NO_x concentrations and F_V/F_M increased with depth, coincident with a decreasing C/N ratio, this suggested that nitrogen limitation was somewhat relieved at the depth of the maximal fluorescence, possibly allowing for the transition between a *Synechoccocus*-dominated cyanobacterial community to a *Prochlorococcus*-dominated community at depth. Such trend in cyanobacteria distribution in relation to NO_x concentration has been previously observed in the North Tasman Sea (Ellwood et al. 2013).

The Australian continent is a significant source of iron-rich dust delivered to the North Tasman Sea, the SAZ and the Southern Ocean (Hesse 1994; Hesse 1997; Gabric et al. 2002; Hesse and McTainsh 2003; Boyd et al. 2004; Bowie et al. 2009; Mongin et al. 2011, Cropp et al. 2013). Periodic inputs of dust laden with iron is thought to stimulate phytoplankton growth (Bowie et al. 2009; Moore et al. 2009), resulting in a shift of the dominant phytoplankton species composition and an increase in carbon fixation (Lenes 2001), thus providing a vital link in the planet's climate control system and being part of a key climate feedback loop linking the lithosphere, atmosphere and ocean (Jickells et al.

2005). In the study region, Moore et al. (2002) model runs, in the absence of, and with, iron-saturating dust deposition scenarios, showed that dust input can increase primary productivity, phytoplankton biomass and induce a shift in the composition of the phytoplankton community. Conflicting results were obtained from recent simulations of wet and dry dust deposition in the North Tasman Sea, with enhanced N_2 fixation by unicellular cyanobacteria (Law et al. 2011) and no effect on phytoplankton growth (Ellwood et al. 2013). During the PINTS study, experiments simulating dry Australian dust deposition, showed that such an event can induce phytoplankton growth and a clear shift in the composition of the phytoplankton community both at P1 and P3 (Hassler et al. unpublished data), suggesting that iron released from dust could affect the structure of the phytoplankton community in our study. This highlights, as observed for artificial large scale Fe fertilisation, the importance of the oceanography and biological conditions at the time of dust deposition (Boyd et al. 2007; Cropp et al. 2013).

Here, differences in dFe: POC, pFe: POC, dFe; Chl *a*, and pFe: Chl *a* between sites and depths, suggested differences in the iron biological requirement or limitation for the in-situ phytoplankton community. The fact that ratios with dFe are smaller than ratios with pFe at P3, suggests that the pool of dFe is not enough to sustain further phytoplankton growth at that site. However, the link of these parameters to iron limitation have to be interpreted with care as they can also indicate (1) a phytoplankton species-dependent or light-dependent cellular Chl-*a* content (see Hassler and Schoemann 2009a; Morrissey and Bowler 2012 for discussion), (2) difference in the lithogenic pFe contribution or (3) the detritus contribution to POC and PON. In addition, luxurious iron uptake, in case of episodic iron enrichment (e.g. subsequent to dust deposition) can increase pFe to POC ratio. Indeed surface iron enrichment was observed at P1. Such dFe profile in this region was previously discussed as the result of dust deposition event (Law et al. 2011).

The N_2 fixation process results in a greater iron biological requirement by diazotrophs than most other phytoplankton (Kutska et al. 2003). A 15-fold increase in Fe uptake was calculated due to an increase in N_2 fixation rate by unicellular cyanobacteria in the North Tasman Sea (Law et al. 2011). The N_2 fixation rate observed in the top 50 m at P1 were similar to the rates previously observed in the study region (Law et al. 2011). In such a case, despite high Fe* values (up to 0.29 at 15 m), potential Fe co-limitation could occur in the surface water of P1. Diazotrophs and cyanobacteria are able to efficiently modulate

their iron biological requirement in response to their environment and during the diel cycle through the control of biological processes (e.g., photosynthesis, N_2 fixation) and gene expression (Saito et al. 2011; Morrissey and Bowler 2012). At the depth of maximal fluorescence, dFe and pFe were extremely low, at a level usually limiting the growth of most eukaryotic phytoplankton (e.g., Sunda and Huntsman 2000, Sarthou et al. 2005; Sedwick et al. 2007) and Fe* was negative indicating probable Fe limitation (Bowie et al. 2009). In addition, dFe: POC were smaller than pFe: POC. Finally, iron bioaccumulation data, suggested a low iron requirement for cyanobacteria relative to eukaryotic phytoplankton at that depth. Indeed iron internalisation constants (data not shown) demonstrated that cyanobacteria (picoplankton) were not iron limited in this case. Primary productivity data demonstrated that light was not limiting the in-situ plankton community at P1, even at the depth of maximal fluorescence. Therefore, our data have demonstrated a vertical difference in nutrient limitation, where in surface waters Fe could limit diazotrophs and nitrate was mostly limiting the growth of other phytoplankton; but at depth iron was the main limiting nutrient for the in-situ eukaryotic phytoplankton. Law et al. (2011) demonstrated that the vertical diffusive supply of nitrate was able to maintain the deep chlorophyll maximum in this region, and that nitrate and possibly low temperature were limiting diazotrophy at these depths. Si concentrations were lower than the average diatom requirement for growth (3.9 ± 5.0 μM; Sarthou et al. 2005), so could also limit diatom abundances and growth at depth.

In the SAZ, the situation is quite different than from the North Tasman Sea. SeaWiFS satellite imagery, model and field observations reveal a persistent phytoplankton bloom present in the surface waters from October to April (Moore et al. 2002; Bowie et al. 2011; de Salas et al. 2011). The earlier SAZ-Sense study performed during the 2007 austral summer demonstrated that this bloom was likely fuelled by episodic, iron-laden dust deposition which may have been transported south in the EAC, and lateral transport from the shelf sediments in EAC eddies (Bowie et al. 2009; Mongin et al. 2011) and the composition of its phytoplankton community was likely influenced by iron availability (Hassler et al. 2012a). However, other in-situ indicators of iron limitation gathered during the SAZ-Sense study such as Fe* (Lannuzel et al. 2011), F_V/F_M (Petrou et al. 2011) and biological uptake of Fe (Schoemann et al., unpublished) suggest that iron is not the main limiting nutrient. Here, as was observed in winter (Ellwood et al. 2008), the strong correlation between Fe and macronutrients concentration demonstrated its role as a

nutrient. The absence of Fe:PO_4 correlation during the SAZ-Sense study (Hassler et al. 2012a), could have been due to dust enrichment in surface waters.

The model developed by Moore et al. (2002) predicts that phytoplankton are mainly limited by Fe with Si co-limitation for diatoms. Despite being in accordance with the potential Fe and Si limitations in the SAZ, our data demonstrated a critical limiting role for light. Primary productivity and in-situ light measurements demonstrated that the primary productivity was strongly limited by the light prevailing at depth of the maximum fluorescence. The plankton biomass in the SAZ region is so high (> 1 μgL^{-1} Chl-*a* in some places; de Salas et al. 2011; this study) that significant shading occurs (Westwood et al. 2011; this study). In the top 30 m, where most of the biomass was observed, most nutrients were strongly depleted due to biological consumption. In this case, Si (0.7 µM), Fe (0.2 nM), NO_x (1.6 – 3.0 µM) were low enough to potentially limit or co-limit further growth of phytoplankton (e.g., Sarthou et al. 2005; Veldhuis et al. 2005; Schoemann et al. 2005; Sedwick et al. 2007). Given that different phytoplankton have different biological requirements for growth (e.g., Ho et al. 2003), a range of co-limiting scenarios might simultaneously occur in the region (Hassler et al. 2012a).

Here F_V/F_M values were below 0.6 at the depth of maximum fluorescence, and pFe: POC were greater than dFe: POC, suggested that dFe is potentially not able to sustain phytoplankton growth. As iron biological requirement of phytoplankton is greater under low light (e.g., Raven et al. 1999; Timmermans et al. 2001), light limitation increase the likelihood of iron co-limitation. In our study, as opposed to the austral summer of 2007 (Bowie et al. 2009; Mongin et al. 2011), no dFe surface enrichment from dust deposition was observed, thus limiting iron inputs needed to sustain phytoplankton growth, as attested by a lower Fe* in surface waters (Bowie et al. 2009). Iron bioaccumulation data suggest that iron limitation will affect the micro, nano and pico-plankton communities differently (this study; Hassler et al. 2012a). For these reasons, it is hard to unequivocally identify the control that nutrient(s) exert on phytoplankton growth in this SAZ region. This study suggests that, in the SAZ southeast of Australia, nutrient limitation is likely to be complex, heterogeneous between phytoplankton groups and size classes, and variable in time due to the evolution of the bloom, as well as nutrient inputs from dust and the mesoscale processes at play in the region (Ellwood et al. 2008b; Bowie et al. 2009; Bowie et al. 2011). In addition, the potential for iron to limit phytoplankton growth is a function of its

complex chemistry and biological requirements, as well as the availability of other nutrients (e.g., N, Si, Cu; see Hassler et al. 2012b; Shaked and Lis 2012; Sunda 2012 for recent reviews). In the SAZ region, light limitation of phytoplankton growth needs to be taken into account during the austral summer.

Acknowledgements:

This research was supported by the Australian Government Cooperative Research Centres Programme through the Antarctic Climate and Ecosystems CRC (ACE CRC), the Australian Research Council (Discovery Projects 1092892 and 110100108), and the Australian Marine National Facility. Hassler was supported by a UTS Chancellor's Fellowship. Law acknowledges funding support from the NZ Ministry of Primary Industries. We are grateful to the captain and crew of RV *Southern Surveyor*; Don McKenzie, Claire Thompson, Gabriel Shaw, Robert van Hale, Mark Baird and Eike Breitbarth for their assistance at sea; Tom Trull and Thomas Rodemann for analysis of POC and PON and comments on previous versions; Malcom Woodward for the determination of NO_x at nanomolar level at P1; Hiski Kippo, Karl Forcey, Alicia Navidad and Sue Reynolds for the determination of macronutrients and other hydrological parameters at sea and calibration of the CTD sensors.

References:

Arrigo, K. R., Robinson, D. H., Worthen, D. L., Dunbar, R. B., DiTullio, G. R., VanWoert, M., and Lizotte, M. P. (1999). Phytoplankton community structure and the drawdown of nutrients and CO_2 in the Southern Ocean. *Science* **283**, 365-367.

Battle, M., Bender, M. L., Tans, P. P., White, J. W. C., Ellis, J. T., Conway, T., and Francey, R. J. (2000). Global carbon sinks and their variability inferred from atmospheric O_2 and δC. *Science* **287**, 2467-2470.

Behrenfeld, M. J., and Falkowski, P. G. (1997). Photosynthetic rates derived from satellite-based chlorophyll concentration. *Limnology and Oceanography* **42**, 1-20.

Behrenfeld, M. J., Worthington, K., Sherrell, R. M., Chavez, F. P., Strutton, P., McPhaden, M. and Shea, D. M. (2006). Controls on Pacific Ocean productivity revealed through nutrient stress diagnostics. *Nature* **442**, 1025-1028.

Behrenfeld, M.J., and Milligan, A. J. (2013). Photophysiological expression of iron stress in Phytoplankton. *Annual Review of Marine Science* **5**, 217-246.

Bertilsson, S., Berglund, O., Karl, D. M., Chisholm, S. W. (2003). Elemental composition of marine *Prochlorococcus* and *Synechococcus*: Implications for the ecological stoichiometry of the sea. *Limnology and Oceanography* **48**, 1721-1731.

Bishop, J. K., Schupack, B. D., Sherrell, R. M., and Conte, M. (1985). A multiple-unit large-volume in-situ filtration system for sampling oceanic particulate matter in mesoscale environments, Adv. Chem. Ser. **209**, 155-175.

Bowen, M., Wilkin, J. L., and Emery, W. J. (2005). Variability and forcing of the East Australian Current, *Journal of Geophysical Res*earch **110**, C03019, doi:10.1029/2004JC002533.

Bowie, A. R., Lannuzel, D., Remenyi, T. A., Wagener, T., Lam, P. J., Boyd, P. W., Guieu, C., Townsend, A. T., and Trull, T. W. (2009). Biogeochemical iron budgets of the Southern Ocean south of Australia: decoupling of iron and nutrient cycles in the subantarctic zone by the summertime supply. *Global Biogeochemical Cycles* **23**, GB4034. doi:10.1029/2009GB003500.

Bowie, A. R., Townsend, A. T., Lannuzel, D., Remenyi, T., and van der Merwe, P. (2010). Modern sampling and analytical methods for the determination of trace elements in marine particulate material using magnetic sector ICP-MS. *Analytica Chimica Acta* **676** 15-27, doi: 10.1016/j.aca.2010.07.037.

Bowie, A. R., Griffiths, F. B., Dehairs, F., and Trull, T. W. (2011). Oceanography of the subantarctic and polar frontal zones south of Australia during summer: setting for the SAZ-Sense study. *Deep-Sea Research II* **58**, 2059–2070.

Boyd, P. W., McTainsh, G., Sherlock, V., Richardson, K., Nichol, S., Ellwood, M. and Frew, R. (2004). Episodic enhancement of phytoplankton stocks in New Zealand subantarctic waters: contribution of atmospheric and oceanic iron supply. *Global Biogeochemical Cycles* **18**, doi:10.1029/2002GB002020.

Boyd, P. W., Jickells, T., Law, C. S., Blain, S., Boyle, E. A., Buesseler, K. O., Coale, K. H., Cullen, J. J., de Baar, H. J. W., Follows, M., Harvey, M., Lancelot, C., Levasseur, M., Owens, N. P. J., Pollard, R., Rivkin, R. B., Sarmiento, J., Schoemann, V., Smetacek, V., Takeda, S., Tsuda, A., Turner, S., and Watson, A. J. (2007). Mesoscale Iron Enrichment Experiments 1993-2005: Synthesis and Future Directions. *Science* **315**, 612-617.

Boyd, P. W., and Ellwood, M. (2010). The biogeochemcial cycle of iron in the ocean. *Nature Geoscience* **3**, 675–682.

Butler, E. C. V., O'Sullivan, J. E., Watson, R. J., Bowie, A. R., Remenyi, T. A., and Lannuzel, D. (2013). Trace metals Cd, Co, Cu, Ni, and Zn in waters of the subantarctic and Polar Frontal Zones south of Tasmania during the 'SAZ-Sense' project. *Marine Chemistry* **148**, 63–76.

Chisholm, S. W. (2000). Stirring times in the Southern Ocean. *Nature* **407**, 685-687.

Cropp, R .A., Gabric, A. J., Levasseur, M., McTainsh, G. H., Bowie, A., Hassler, C. S., Law, C. S., McGowan, H., Tindale, N., and Viscarra Rossel, R. (2013). The likelihood of observing dust-stimulated phytoplankton growth in waters proximal to the Australian continent. *Journal of Marine Systems* **117–118**, 43–52.

Cullen, J. T., and Sherrell, R. M. (1999). Techniques for determination of trace metals in small samples of size-fractionated particulate matter: phytoplankton metals off central California. *Marine Chemistry* **67**, 233-247.

Cullen, J. T., Chase, Z., Coale, K. H., Fitzwater, S. E., and Sherrell, R. M. (2003). Effect of iron limitation on the cadmium to phosphorous ratio of natural phytoplankton assemblages from the Southern Ocean. *Limnology and Oceanography* **48**, 1079-1087.

Cullen, J. T., and Sherrell, R. M. (2005). Effects of dissolved carbon dioxide, zinc, and manganese on the cadmium to phosphorus ratio in natural phytoplankton assemblages. *Limnology and Oceanography* **50**, 1193-1204.

Cutter, G., Andersson, P., Codispoti, L., Croot, P., Fracois, R., Lohan, M., Obata, H., and van der Loeff, M. R. (2010). Sampling and sample handling protocols for GEOTRACES Cruises. www.geotraces.org/libraries/documents/Intercalibration/Cookbook.pdf.

de Baar, H. J. W., van Leeuwe, M. A., Scharek, R., Goeyens, L., Bakker, K. M. J., and Fritsche, P. (1997). Nutrient anomalies in *Fragilariopsis kerguelensis* blooms, iron deficiency and the nitrate/phosphate ratio (A. C. Redfield) of the Antarctic Ocean. *Deep-Sea Research II* **44**, 229-260.

De Jong, J.T.M., J. den Das, U. Bathmann, M.H.C. Stoll, G. Kattner, R.F. Nolting and H.J.W. de Baar. (1998). Dissolved iron at sub-nanomolar levels in the Southern Ocean as determined by shipboard analysis. *Analytica Chimica Acta* **377**, 113-124.

de Salas, M. F., Eriksen, R., Davidson, A. T., and Wright, S. W. (2011). Protistan communities in the Australian sector of the Sub-Antarctic zone during SAZ-Sense. *Deep-Sea Research II* **58**, 2135–2149.

Doblin, M. A., Ralph, P. J., Petrou, K. L., Shelly, K., Westwood, K., van den Enden, R., Wright, S., Griffiths, B. (2011). Diel variation of chl-a fluorescence, phytoplankton pigments and productivity in the Sub-Antarctic Zone. *Deep Sea Research II***58**, :2189-2199. doi : 10.1016/j.dsr2.2011.05.021.

Ellwood, M. J. (2008)a. Wintertime trace metal (Zn, Cu, Ni, Cd, Pb and Co) and nutrient distributions in the Subantarctic Zone between 40–52°S; 155–160°E. *Marine Chemistry* **112**, 107-117.

Ellwood, M. J., Boyd, P. W., and Sutton, P. (2008)b.Winter-time dissolved iron and nutrient distributions in the subantarctic zone from 40–52 ^{0}S;155–160 ^{0}E. *Geophysical Research Letters* **35**, L11604.doi:10.1029/2008GL033699.

Ellwood, M. J., Law, C. S., Hall, J., Woodward, E. M. S., Strzepek, R., Kuparinen, J., Thompson, K., Pickmere, S., Sutton, P., and Boyd, P. W. (2013). Relationships between nutrient stocks and inventories and phytoplankton physiological status along an oligotrophic meridional transect in the Tasman Sea. *Deep Sea Research I* **72**, 102-120.

Finkel, Z. V., Quigg, A. S., Chiampi, R. K., Schofield, O. E., and Falkowski, P. G. (2007). Phylogenetic diversity in cadmium : phosphorus ratio regulation by marine phytoplankton. *Limnology and Oceanography* **52**, 1131-1138.

Finkel, Z. V., Beardall, J., Flynn, K. J., Quigg, A., Rees, T. A. V., and Raven, J. A. (2010). Phytoplankton in a changing world: cell size and elemental stoichiometry. *Journal of Plankton Research* **32**, 119-137.

Gabric, A. J., Cropp, R., Ayers, G. P., McTainsh, G. and Braddock, R. (2002). Coupling between cycles of phytoplankton biomass and aerosol optical depth as derived from SeaWiFS time series in the Subantarctic Southern Ocean. *Geophysical Research Letters* **29**, 1112, 10.1029/2001GL013545.

Gault-Ringold, M., Adu, T., Stirling, C. H., Frew, R. D., and Hunter, K. A. (2012). Anomalous biogeochemical behavior of cadmium in subantarctic surface waters: mechanistic constraints from cadmium isotopes. *Earth and Planetary Science Letters* **341–344**, 94–103.

GEOTRACES Science Plan (2006). An international study of the marine biogeochemical cycles of trace elements and their isotopes. Scientific Committee on Oceanic Research, Baltimore, MD, USA.

Godfrey, J. S., Cresswell, G. R., Golding, T. J., Pearce, A. F., and Boyd, R. (1980). The separation of the East Australian Current, *Journal of Physical Oceanography* **10**, 430-440.

Hassler, C. S., and Schoemann, V. (2009)a. Bioavailability of organically bound Fe to model phytoplankton of the Southern Ocean. *Biogeosciences* **6**, 2281-2296.

Hassler, C. S., and Schoemann, V. (2009)b. Discriminating between intra- and extracellular metals using chemical extractions-the case of iron. *Limnology and Oceanography Methods* **7**, 479-489.

Hassler, C. S., Sinoir, M., Clementson, L. A., and Butler, E. C. V. (2012)a. Exploring the link between micro-nutrients and phytoplankton in the Southern Ocean during the 2007 autral summer. *Frontiers in Microbiology* **3**, article 202, 1-26.

Hassler, C. S., Schoemann, V., Boye, M., Tagliabue, A., Rozmarynowycz, M., McKay, R. M. L. (2012)b. Iron Bioavailability in the Southern Ocean. In 'Oceanography and Marine Biology: An annual review: Vol. 50' (Eds R. N. Gibson, R. J. A. Atkinson, J. D. M. Gordon, and R. N. Hughes). pp. 1-64. (CRC Press, New York).

Hesse, P. P. (1994). The record of continental dust from Australia in Tasman Sea Sediments. *Quaternary Science Reviews* **13**, 257-272.

Hesse, P. P. (1997). Mineral magnetic 'tracing' of aeolian dust in southwest Pacific sediments. *Palaeogeography Palaeoclimatology Palaeoecology* **131** 327-353.

Hesse, P. P., and McTainsh, G. H. (2003). Australian dust deposits: modern processes and the Quaternary record. *Quaternary Science Reviews* **22**, 2007-2035.

Ho, T. Y., Quigg, A., Finkel, Z. V., Milligan, A. J., Wyman, K., Falkowski, P. G., and Morel, F. M. M. (2003). The elemental composition of some marine phytoplankton. *Journal of Phycology* **39**, 1145-1159.

Hobday, A, Poloczanska, E. S., and Matear, R. J. (2008). Implications of climate change for Australian fiecheries and acquaculture: A preliminary assessment. Report to the Australian Greenhouse Office.

Hutchins, D. A., and Bruland, K. W. (1998). Iron-limited diatom growth and Si:N uptake ratios in a coastal upwelling regime. *Nature* **393**, 161-164.

IPCC, 2007. The Physical Science Basis. Contribution of Working Group 1 to the Fourth Assessment Report of the Intergovernmental Panel on Climate Change. (Eds S. Solomon, D. Qin, M. Manning, Z. Chen, M.C. Marquis, K. Averyt, M. Tignor and H.L. Miller). Intergovernmental Panel on Climate Change, Cambridge and New York.

Jacquet, S. H. M., Lam, P. J., Trull, T. W., and Dehairs, F. (2011). Carbon export production in the Sub-Antarctic zone and Polar Front Zone south of Tasmania. *Deep-Sea Research II* **58**, 2277–2292.

Jeffrey, S. W., and Wright, S. W. (2006). Photosynthetic pigments in marine microalgae: insights from cultures and the sea. In 'Algal Cultures, Analogues of Blooms and Applications'. (Ed. D. V. Subba Rao). pp. 33-90. (Enfield, NH, Science Publishers).

Jickells, T. D., An, Z. S., Anderson, K. K., Baker, A. R., Bergametti, G., Brooks, N.,Cao, J. J., Boyd, P. W., Duce, R. A., Hunter, K. A., Kawahata, H., Kubilay, N., laRoche, J., Liss, P. S., Mahowald, N., Prospero, J. M., Ridgwell, A. J., Tegen, I., and Torres, R. (2005). Global iron connections between desert dust, ocean biogeochemistry, and climate. *Science* **308**, 67-71.

Johnson, K. M., Dickson, A. G., Eischeid, G., Goyet, C., Guenther, P., Key, R. M., Millero, F. J., Purkerson, D., Sabine, C. L., Schottle, R. G., Wallace, D. W. R., Wilke, R. J., and Winn, C. D. (1998). Coulometric total carbon dioxide analysis for marine studies: assessment of the quality of total inorganic carbon measurements made during the US Indian Ocean CO_2 Survey 1994–1996. *Marine Chemistry* **63**, 21-37.

Johnson, K. S., Boyle, E., Bruland, K., Coale, K., Measures, C., Moffett, J., Aguilar-Islas, A., Barbeau, K., Bergquist, B., Bowie, A., Buck, K., Cai, Y., Chase, Z., Cullen, J., Doi, T., Elrod, V., Fitzwater, S., Gordon, M., King, A., Laan, P., Laglera-Baquer, L., Landing, W., Lohan, M., Mendez, J., Milne, A., Obata, H., Ossiander, L., Plant, J., Sarthou, G., Sedwick, P., Smith, G. J., Sohst, B., Tanner, S., Van den Berg, S., Wu, J. 2007. The SAFe Iron Intercomparison Cruise: An International Collaboration to Develop Dissolved Iron in Seawater Standards. *Eos, Transactions, American Geophysical Union* **88**, 131-132.

Karl, D.M. (2000). Phosphorus, the staff of life. *Nature* **406**, 31-32.

King, P., Kennedy, H., Newton, P., Jickells, T., Timothy Brand, T., Calvert, S., Cauwet, G., Etcheber, H., Head, B., Khripounoff, A., Manighetti, B., and Miquel, J. C. (1998). Analysis of total and organic carbon and total nitrogen in settling oceanic particles and marine sediment: an interlaboratory comparison. *Marine Chemistry* **60**, 203-216.

Kustka, A. B., Sanudo-Wilhelmy, S. A., Carpenter, E. J., Capone, D., Burns, J. and Sunda, W. G. (2003). Iron requirements for dinitrogen- and ammonium-supported growth in cultures of Trichodesmium (IMS 101): Comparison with nitrogen fixation rates and iron: carbon ratios of field populations. *Limnology and Oceanography* **48**, 1869-1884.

Law, C. S., Ellwood, M., Woodward, E. M. S., Marriner, A., Bury, S., and Safi, K. (2011). Response of surface nutrient inventories and nitrogen fixation to a tropical cyclone in the South-West Pacific. *Limnology and Oceanography* **56**, 1372–1385.

Lannuzel, D., Remenyi, T., Lam, P. J., Townsend, A., Ibisanmi, E., Butler, E., Wagener, T., Schoemann, V., and Bowie, A. R. (2011). Distributions of dissolved and particulate iron in the Sub-Antarctic and Polar Frontal Southern Ocean (Australian sector). *Deep-Sea Research II* **58**, 2094–2112.

Leblanc, K., Hare, C. E., Boyd, P. W., Bruland, K. W., Sohst, B., Pickmere, S., Lohan, M. C., Buck, K., Ellwood, M., and Hutchins, D. A. (2005). Fe and Zn effects on the Si cycle and diatom community structure in two contrasting high and low-silicate HNLC areas. *Deep-Sea Research I* **52**, 1842-1864.

Lenes, J. M., Darrow, P. D., Cattrall, C., Heil, C. A., Callahan, M., Vargo, G. A., Byrne, R. H., Prospero, J. M., Bates, D. E., Fanning, K. A., and Walsh, J. J. (2001). Iron fertilization and the *Trichodesmium* response on the West Florida shelf. *Limnology and Oceanography* **46**, 1261-1277.

Lewis, M. R., and Smith, J. C. (1983). A small volume, short-incubation-time method for measurement of photosynthesis as a function of incident irradiance. *Marine Ecology Progress Series* **13**, 99-102.

Marie, D., Partensky, F., Jacquet, S., and Vaulot, D. (1997). Enumeration and cell cycle analysis of natural populations of marine picoplankton by flow cytometry using the nucleic acid stain SYBR Green. *Applied Environmental Microbiology* **63**,186-193.

Martin, J. H., Gordon, R. M., and Fitzwater, S. E. (1990). Fe in Antarctic waters. *Nature* **345**, 156-158.

Mongin, M., Matear, R., and Chamberlain, M. (2011). Seasonal and spatial variability of remotely sensed chlorophyll and physical fields in the SAZ-Sense region. *Deep-Sea Research II* **58**, 2082–2093.

Moore, J. K., and Abbott, M. R. (2000). Phytoplankton chlorophyll distributions and primary production in the Southern Ocean. *Journal of Geophysical Research* **105**, C12, 28709 –28722.

Moore, J. K., Doney, S. C., Glover, D. M., and Fung, I. Y. (2002). Iron cycling and nutrient-limitation patterns in surface waters of the World Ocean. *Deep-Sea Research II* **49**, 463–507.

Moore, J. K., and Doney, S.C. (2007). Iron availability limits the ocean nitrogen inventory stabilizing feedbacks between marine denitrification and nitrogen fixation. *Global Biogeochemical Cycles* **21**, GB2001, doi:10.1029/2006GB002762.

Moore, C. M., Mills, M. M., Achterberg, E. P., Geider, R. J., La Roche, J., Lucas, M. I., McDonagh, E. L., Pan, X., Poulton, A. J., Rijkenberg, M. J. A., Suggett, D. J., Ussher, S. J., and Woodward, E. M. S. (2009). Large-scale distribution of Atlantic nitrogen fixation controlled by iron availability. *Nature Geoscience* **2**, 867-871.

Mohr, W., Großkopf, T., Wallace, D. W. R., and LaRoche, J. (2010). Methodological Underestimation of Oceanic Nitrogen Fixation Rates. *PLoS ONE* **5,** e12583. doi:10.1371/journal.pone.0012583.

Montoya, J. P., Voss, M., Kahler, P., and Capone, D. G. 1996. A simple, high-precision, high-sensitivity tracer assay for N-2 fixation. *Applied Environmental Microbiology* **62**, 986–993.

Morel, F. M. M., and Price, N. M. (2003). The biogeochemical cycles of trace metals in the oceans. *Science* **300**, 944-947.

Morrissey, J. C., and Bowler, C. (2012). Iron utilization in marine cyanobacteria and eukaryotic algae. *Frontiers in Microbiology***3**, article 43: 1-13.

Nilsson, C. S., and Cresswell, G. R. (1981). The formation and evolution of East Australian Current warm core eddies, *Progress in Oceanography* **9**, 133-183.

Nuester, J., Vogt, S., Newville, M., Kustka, A. B., and Twining, B. S. (2012). The unique biogeochemical signature of the marine diazotroph Trichodesmium. *Frontiers in Microbiology* **3**, article 150: 1-15.

Obata, H. , H. Karatani and E. Nakayama. (1993). Automated determination of iron in seawater by chelating resin concentration and chemiluminescence detection. *Analytical Chemistry* **65**, 1524-1528.

Orsi, A. H., Whitworth III, T. W., and Nowlin, W. D. (1995), On the meridional extent and fronts of the Antarctic Circumpolar Current, *Deep-Sea Research I* **42**, 641-673.

O'Sullivan, J. E., Watson, R. J., and Mackey, D .J. (1995). A guide to trace metal sampling in estuarine waters. In Australian Marine Data Collection and Management Guidelines Workshop, 5–6 December 1995, CSIRO Marine Laboratories, Hobart, Tasmania (Canberra, ACT: Australian Dept. of the Environment Sport and Territories).

O'Sullivan, J. E., Watson, R. J. and Butler, E. C. V. (2013). An ICP-MS procedure to determine Cd, Co, Cu, Ni, Pb and Zn in oceanic waters using in-line flow-injection with solid-phase extraction for preconcentration. *Talanta,* submitted.

Parekh, P., Follows, M. J., and Boyle, E. A. (2005), Decoupling of iron and phosphate in the global ocean. *Global Biogeochemical Cycles* **19**, GB2020, doi:10.1029/2004GB002280.

Pearce, I., Davidson, A. T., Thomson, P., Wright, S. W., and van den Enden, R. (2011). Marine microbial ecology in the Sub-Antarctic Zone: rates of bacterial and phytoplankton growth and grazing by heterotrophic protists. *Deep-Sea Research II* **58**, 2248–2259.

Petrou, K. L., Hassler, C. S., Doblin, M. A., Shelly, K., Schoemann, V., and Ralph, P. J. (2011). Interaction of iron and light on Southern Ocean phytoplankton. *Deep-Sea Research II* **58**, 2200-2211.

Quigg, A., Finkel, Z. V., Irwin, A. J., Rosenthal, Y., Ho, T. Y., Reinfelder, J. R., Schofield, O., Morel, F. M. M., and Falkowski, P. G. (2003). The evolutionary inheritance of elemental stoichiometry in marine phytoplankton. *Nature* **425**, 291-294.

Raven, J.A., Evans, M.C.W., and Korb, R.E. (1999). The role of trace metals in photosynthetic electron transport in O_2-evolving organisms. *Photosynthesis Research* **60**, 111-149.

Redfield, A. C., Ketchum, B. H., and Richards, F. A. (1963). The influence of organisms on the composition of sea-water. In The composition of seawater. Comparative and descriptive oceanography. The sea: ideas and observations on progress in the study of the seas, vol. 2, (Ed. M. N. Hill) pp. 26-77. (Interscience, New York).

Reynolds, S., and Navidad, A. (2012). SS2010/01 - Role of iron and other micronutrients in controlling primary productivity in the Tasman Sea: bioavailability, biogeochemical cycling and sources. CSIRO Marine national Facility, unpublished voyage hydrochemistry report, October 2012, Hobart, Tasmania.

Ridgway, K. R., Dunn, J. R., and Wilkin, J. L. (2002) Ocean interpolation by four-dimensional least squares -Application to the waters around Australia. *Journal of Atmospheric and Oceanic Technology* **19**, 1357-1375.

Ridgway, K. R., and Dunn, J. R. (2003). Mesoscale structure of the mean East Australian Current System and its relationship with topography, *Progress in Oceanography* **56**, 189-222.

Ridgway, K. R., and Dunn, J. R. (2007) Observational evidence for a Southern Hemisphere oceanic 'Supergyre'. *Geophysical Research Letters* **34**, L13612, doi:10.1029/2007GL030392.

Ridgway, K. R. (2007). Seasonal circulation around Tasmania: An interface between eastern and western boundary dynamics. *Journal of Geophysical Research* **112**, C10016, doi:10.1029/2006JC003898.

Ridgway, K. R., Coleman, R. C., Bailey, R. J., and Sutton, P. (2008). Decadal variability of East Australian Current transport inferred from repeated high-density XBT transects, a CTD survey and satellite altimetry, Journal of Geophysical Research **113**, C08039,doi:10.1029/2007JC004664.

Saito, M. A., Bertrand, E. M., Dutkiewicz, S., Bulygin, V. V., Moran, D. M., Monteiro, F. M., Follows, M. J., Valois, F. W., and Waterbury, J. B. (2011). Iron conservation by reduction of metalloenzyme inventories in the marine diazotroph *Crocosphaera watsonia*. *Proceedings of the National Academy of Sciences of the United States of America* **108**, 2184-2189.

Sarthou, G., Timmermans, K., Blain, S., and Tréguer, P. (2005). Growth physiology and fate of diatoms in the ocean: A review. *Journal of Sea Research* **53**, 25-42.

Schoemann, V., Becquevort, S., Stefels, J., Rousseau, V., and Lancelot, C. (2005). *Phaeocystis* blooms in the global ocean and their controlling mechanisms: a review. *Journal of Sea Research* **53**, 43–66.

Schreiber, U. 2004. Pulse-Amplitude-Modulated (PAM) Fluorometry and Saturation Pulse Method, p. 279-319. *In* G. G. Papagiorgiou [ed.], Advances in photosynthesis and respiration. Springer.

Sedwick, P. N., Garcia, N. S., Riseman, S. F., Marsay, C. M., and DiTullio, G.R. (2007). Evidence for high iron requirements of colonial *Phaeocystis antarctica* at low irradiance. *Biogeochemistry* **83**, 83-97.

Seymour, J. R., Doblin, M. A., Jeffries, T. C., Brown, M. V., Newton, K., Ralph, P. J., Baird, M., Mitchell, J. G. (2012). Contrasting microbial assemblages in adjacent water-masses associated with the East Australian Current. *Environmental Microbiology Reports* **4**,548-555; DOI: 10.1111/j.1758-2229.2012.00362.x.

Shaked, Y., and Lis, H. (2012). Disassemblingironavailabilitytophytoplankton *Frontiers in Microbiology* **3**, article 123: 1-26.

Sokolov, S., and Rintoul, S. R. (2000). Circulation and water masses of the southwest Pacific: WOCE section P11, Papua New Guinea to Tasmania. *Journal of Marine Res*earch **58**, 223-268.

Sunda, W. G., and Huntsman, S. A. (2000). Effect of Zn, Mn, and Fe on Cd accumulation in phytoplankton: implications for oceanic Cd cycling. *Limnology and Oceanography* **45**, 1501-1516.

Sunda, W. G. (2012). Feedback interactions between trace metal nutrients and phytoplankton in the ocean. *Frontiers in Microbiology* **3**, article 204: 1-22.

Timmermans, K. R., Davey, M. S., Van der Wagt, B., Snoek, J., Geider, R. J., Veldhuis, M. J. W., Gerringa, L. J. A., and de Baar, H. J. W. (2001). Co-limitation by iron and light of *Chaetoceros brevis, C. dichaeta and C. calcitrans* (Bacillariophyceae). *Marine Ecology Progress Series* **217**, 287-297.

Townsend, A. T. (2000). The accurate determination of the first row transition metals in water, urine, plant, tissue and rock samples by sector field ICP-MS, *Journal of Analytical Atomic Spectrometry* **15**, 307-314.

Twining, B. S., Baines, S. B., and Fisher, N. S. (2004). Element stoichiometries of individual plankton cells collected during the Southern Ocean Iron Experiment (SOFeX). *Limnology and Oceanography* **49**, 2115-2128.

Van Heukelem, L., and Thomas, C. (2001). Computer assisted high-performance liquid chromatography method development with applications to the isolation and analysis of phytoplankton pigments. *Journal of Chromatography A*. **910**, 31-49.

Veldhuis, M., Timmermans, K., Croot, P., and Vanderwagt, B. (2005). Picophytoplankton, a comparative study of their biochemical composition and photosynthetic properties. *Journal of Sea Research* **53**, 7-24.

Westwood, K. J., Griffiths, F. B., Webb, J. P., and Wright, S. W. (2011). Primary production in the Sub-Antarctic and Polar Frontal zones south of Tasmania, Australia; SAZ-Sense survey, 2007. *Deep-Sea Research II* **58**, 2162–2178.

Figure captions:

Figure 1: The Tasman Sea region showing the bottom topography (depth, [m]). The PINTS stations along the cruise track are shown by the coloured symbols. Transect stations are shown in yellow, process stations in red (P1=Stn 5, P2=Stn 9, P3=Stn 12) and reoccupation of the process station 3 from the SAZ-Sense expedition (*Aurora Australis*, Jan-Feb 2007) in green (SAZ=Stn14). Thicker solid lines indicate the East Australian Current (EAC), Tasman Front (TF), and EAC Extension. The dashed line represents the path of the Subtropical Front (STF).

Figure 2: (a) Surface circulation of the Tasman Sea region as shown by the surface steric height field ($h_{0/200}$, m) obtained from the CARS climatology (Ridgway and Dunn, 2003). (b) The surface height variability (m) obtained from 18 years of satellite altimetry observations. (c) The full-depth transport shown by the depth-averaged steric height from CARS.

Figure 3: Temperature anomaly data (with respect to the annual mean from CARS) obtained from synTS along the PINTS cruise track in the upper 1000 m (a). Temperature anomaly from CTD stations (b). Note the increased resolution in the vertical axis from 0-125 m. The location of the CTD stations is indicated by the dashed lines and the end of each transect is shown by the full lines.

Figure 4: Temperature (a) and salinity (b) at 60-m inferred from SynTS. Temperature (c) and salinity (d) at 250 m inferred from SynTS. The contour intervals are 0.25°C (a, c); 0.025 (b) and 0.02 (d) g kg^{-1}. The upper panels show the pattern for the first portion of the voyage (January 2010) and the lower panels represent the latter half of the voyage (February 2010).

Figure 5: CTD data collected, (a) temperature in °C, (b) salinity in g kg^{-1} and (c) oxygen in µM down to 1000m along the PINTS voyage track. The voyage track is shown on the right panel overlaid on bathymetry.

Figure 6: Phosphate (PO_4, a), nitrate + nitrite (NOx, b) and silicic acid (Si, c) distribution along the PINTS voyage track down to 1000 m depth. The voyage track is shown on the right panel overlaid on bathymetry.

Figure 7: Total Chlorophyll-*a* (Tot Chl-*a*, a) and particulate organic carbon to particulate nitrogen ratio (C/N, b) along the PINTS voyage track. Tot Chl-*a* distribution is shown down to 125 m, whereas C/N are shown for surface (25m) and the depth of maximum fluorescence. The depth of maximum fluorescence coincides with the depth of maximum Tot Chl-*a*. The voyage track is shown in the right panel, overlaid on bathymetry.

Figure 8: Profile of dissolved trace elements and nutrients at sites P1 (Stn5, full circles) and P3 (Stn 12, empty circles). Dissolved iron (dFe, a), cadmium (dCd, b), silicic acid (Si, c), nitrate + nitrite (NO_x, d), and phosphate (PO_4, e).

Figure 9: Disappearance ratios for Cd (panel a), nitrate + nitrite (NO_X, b), and Fe (panels c to h) at sites P1 (Stn 5, full circles) and P3 (Stn 12, empty circles). Disappearance ratio are shown against phosphate (PO_4, panels a-d), silicic acid (Si, panels e-f), and nitrate + nitrite (NO_X, panels g-h). Disappearance ratios are calculated by linear regression (slope with 95 % confidence interval and coefficient of correlation) using data down to 4000 m (panels a-c, e, g) and down to 125m (panels d, f, h). NA = not applicable.

Figure 10: Biological parameters from sites P1 and P3. Maximum quantum yields from the whole phytoplankton community (F_V/F_M Blue, full circles) and from cyanobacteria (F_V/F_M Red, empty circles) are shown in panels a and e (*n*=3, error bars represents the standard deviation); cell abundance are shown in panels b and f; total chlorophyll-*a* (Tot Chl-*a*) is shown in panel d; biomarker pigments are shown in panels c and g; and N_2 fixation arte are shown in panel h (*n*=3,error bars represents the standard deviation).

Figure 11: Iron bioavailability of size fractionated phytoplankton community from the depth of maximum fluorescence at stations P1 and P3. Average iron uptake rates are presented with half interval (*n*= 2, panel a and c). Size fractionated total Chlorophyll-*a* (Tot Chl-*a*, b) and biomarker pigments relative concentration (c) is presented for microplankton (> 10 µm), nanoplankton (2-10 µm) and picoplankton (0.7-2 µm).

Figure 12: Biological carbon fixation by phytoplankton at sites P1 and P3 for two depths (surface, 15m and maximum of fluorescence (P1= 125m, P3 = 25m). Carbon fixation is shown at two light intensities (30 ± 3 and 271 ± 35 μmol photons m^{-2} s^{-1}, *n*=6, represented in dark and light bars respectively). Optimal carbon fixation was calculated from in-situ temperature (open stars) using the equation from Behrenfeld and Falkowski (1997). Error bars represent half interval (*n*=2).

1

Table 1: Stations coordinates and dates for the PINTS expedition. Activities are physical oceanography (O), nutrients (N), Biology (B), Trace metals (TM), Process study (P). Full water column (0-4500m) sampling is indicated by an asterisk, otherwise 0-1000m were sampled when bottom depth was > 1000 m. A single time of sampling was not appropriate at process stations (P1, P2, P3 and reoccupation from the SAZ-Sense voyage (2007)) as 3 to 17 CTD casts and 2 to 7 trace metal rosette casts were performed.

Stns #	Activity	Latitude (⁰E)	Longitude (°S)	Date (UTC, 2010)	Time (UTC)
1	O, N, B	153 5	33 2	23-Jan	0:49
2	O, N, B, TM	155 5	32 5	24-Jan	17:12
3	O, N, B, TM	158 4	32 0	26-Jan	1:02
4	O, N, B, TM	161 5	31 0	26-Jan	19:49
5 - P1	O, N, B, TM, P*	165 0	30 0	27 to 31-Jan	NA
6	O, N, B, TM	164 3	31 4	31-Jan	22:55
7	O, N, B	163 3	35 3	2-Feb	2:26
8	O, N, B, TM	162 4	38 3	3-Feb	1:13
9 - P2	O, N, B, TM, P*	162 1	39 6	3 to 4-Feb	NA
10	O, N, B, TM	161 1	42.3	6-Feb	18:19
11	O, N, B	160 5	43 5	7-Feb	7:41
12 - P3	O, N, B, TM, P*	159 5	46 2	7 to 9-Feb	NA
13	O, N, B, TM	156 5	46 0	10-Feb	22:54
14 - SAZ	O, N, B, TM*	153 2	45 6	11 to12-Feb	NA
15	O, N, B, TM	150 5	45 5	13-Feb	16:05
16	O, N, B, TM	149 4	44 6	14-Feb	1:57
17	O, N, B, TM	148 4	44 1	14-Feb	13:12
18	O, N, B, TM	148 0	43 4	14-Feb	23:10

Table 2: Particulate data collected by Mc Lane pumps on a 1 µm quartz filter. Particulate iron (pFe), organic carbon (POC) and particulate nitrogen (PON) from surface water and the depth of maximal fluorescence (F max) at P1 and P3. For comparison, similar data considering the dissolved iron (dFe, < 0.2 µm) and total chlorophyll-*a* (Chl-*a*) are shown.

	pFe (nM)	C/N	pFe/POC (nmol:µmol)	pFe/Chl-*a* (nmol:µg)	Chl-*a*/POC (µg:µmol)	dFe/POC (nmol:µmol)	dFe/Chl-*a* (nmol:µg)
P1							
Surface (30 m)	0.23	8.95	0.12	0.11	0.06	0.12	1.90
F max (95m)	0.12	6.52	0.08	0.39	0.24	0.03	0.61
P3							
F max (30 m)	0.77	6.61	0.15	1.11	0.14	0.04	0.30

Primary productivity induced by iron and nitrogen in the Tasman Sea – An overview of the PINTS expedition.

C.S. Hassler[1, 2, 3*]; K. R. Ridgway[2]; A. R. Bowie[4, 5]; E.C.V. Butler[2, #]; L. A. Clementson[2]; M. A. Doblin[1]; D. M. Davies[2]; C. Law[6]; P. J. Ralph[1]; P. van der Merwe[4]; R. Watson[2]; M. J. Ellwood[7]

[1] Plant Functional Biology and Climate Change Cluster, University of Technology Sydney, PO Box 123, Broadway, 2007, NSW, Australia.

[2] CSIRO Wealth from Oceans Research Flagship, and CSIRO Marine and Atmospheric Research, Castray Esplanade, Hobart, 7000, TAS, Australia.

[3] Institute F.-A. Forel, University of Geneva, 10 rte de Suisse, 1290 Versoix, Switzerland.

[4] Antarctic Climate & Ecosystems Co-operative Research Centre, University of Tasmania, Private Bag 80, Hobart, 7001, TAS, Australia.

[5] Institute for Marine and Antarctic Studies, University of Tasmania, Private Bag 129, Hobart, TAS 7001, Australia.

[6] National Institute of Water and Atmospheric Research (NIWA), 301 Evans Bay Parade, Greta Point, PO Box 14-901, Kilbirnie, Wellington, New Zealand.

[7] Research School of Earth Sciences, Building 61, Mills Road, Australian National University, Canberra, ACT 0200.

[*]Corresponding author: Christel.Hassler@unige.ch

[#] present address: Australian Institute of Marine Science, Arafura Timor Research Facility, PO Box 41775, Casuarina NT 0811, Australia.

Supplementary Material:

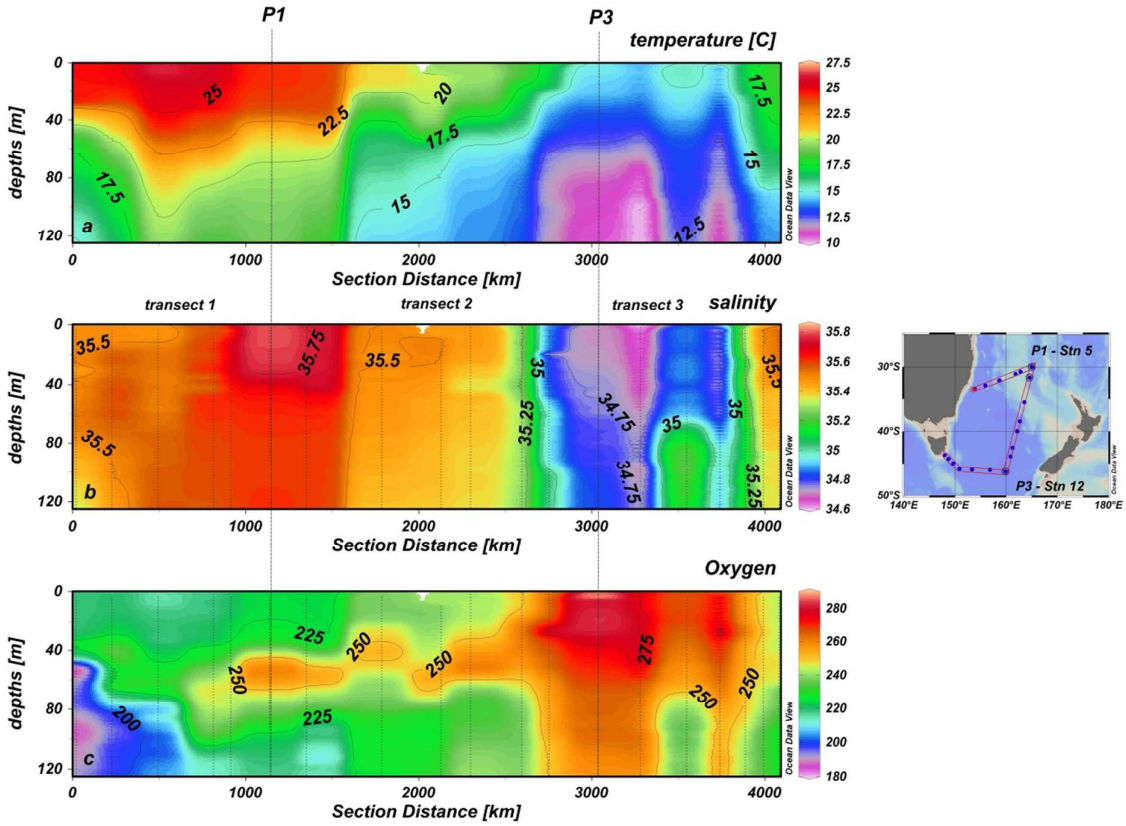

Figure 1: Data collected from the CTD deployment along the PINTS cruise track. Temperature (a), salinity (b) and oxygen (c) are shown down to 125m. This figure focuses on the area where phytoplankton have been measured.

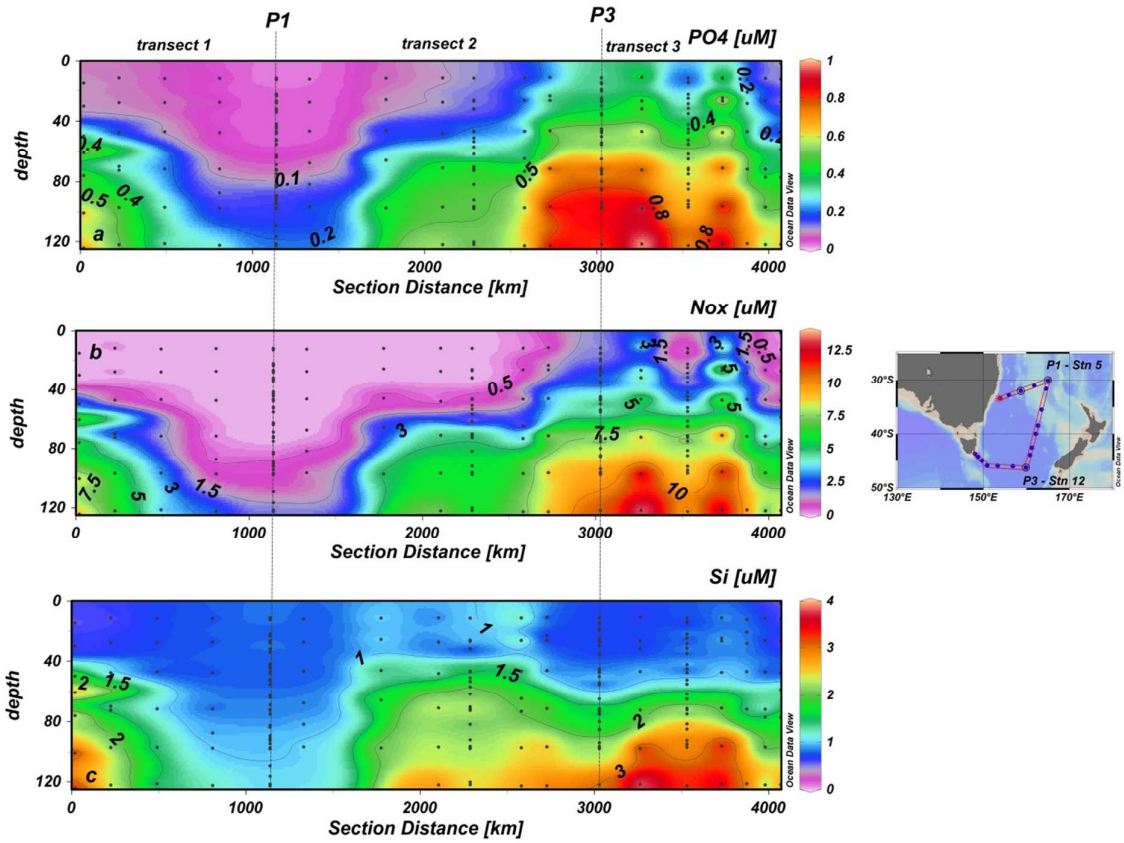

Figure 2: Data collected from the CTD deployment along the PINTS cruise track. Phosphate (PO4, a), nitrate + nitrite (NOx, b) and silicic acid (Si, c) are shown down to 125m. This figure focuses on the area where phytoplankton have been measured.

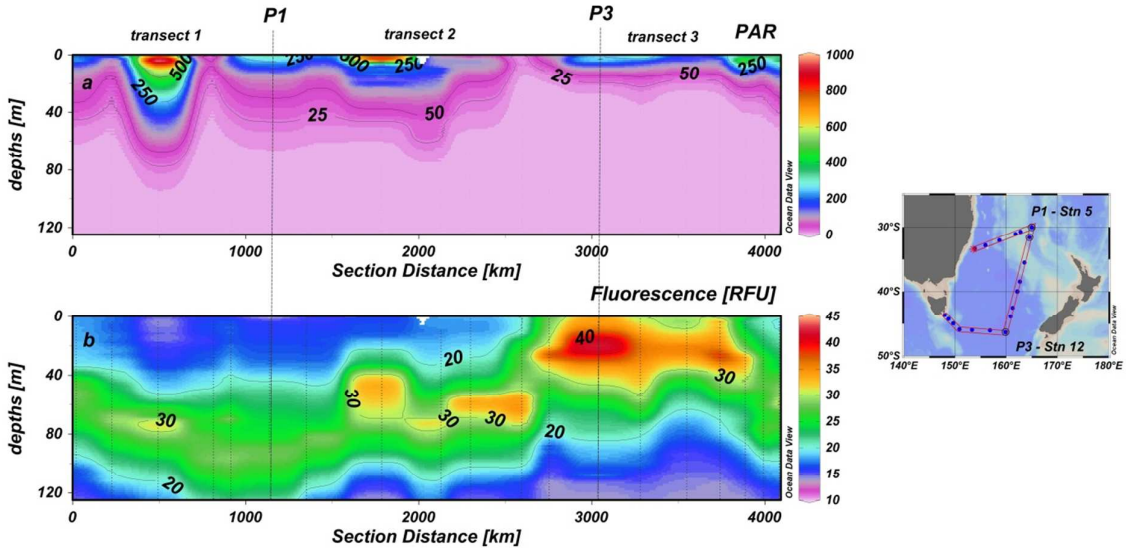

Figure 3: Data collected from the CTD deployment along the PINTS cruise track. Photosynthetic active radation (PAR, a), and fluorescence (b) are shown down to 125m. This figure focuses on the area where phytoplankton have been measured.

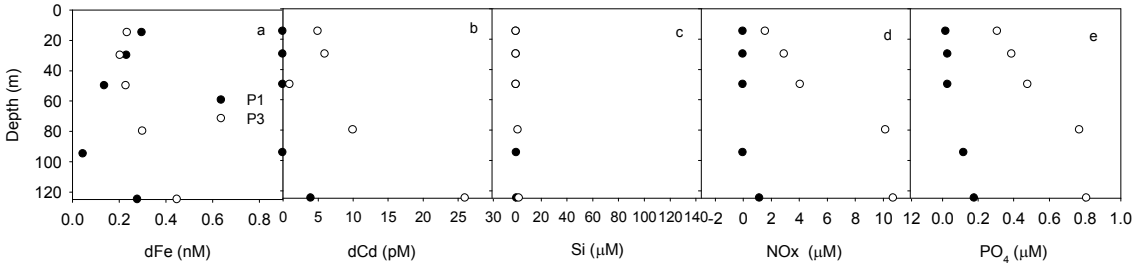

Figure 4: Profile of dissolved trace elements and nutrients in surface waters at sites P1 (full circles) and P3 (empty circles). Dissolved iron (dFe, a), cadmium (dCd, b), silicic acid (Si, c), nitrate + nitrite (NO_x, d), and phosphate (PO_4, e).

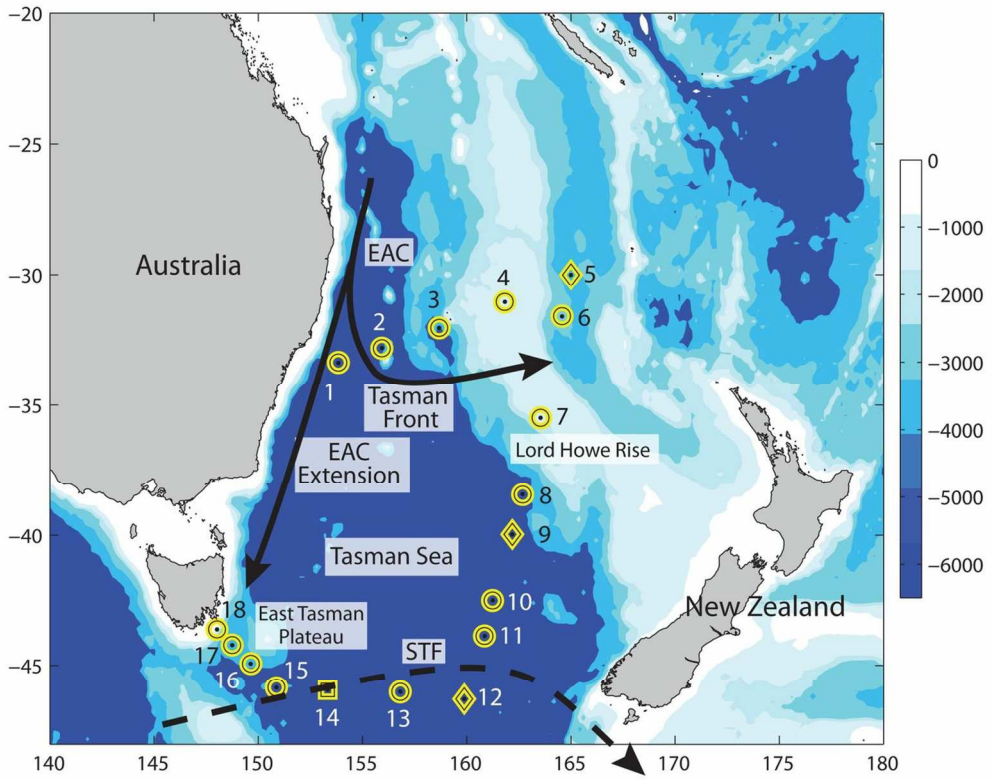

535x423mm (72 x 72 DPI)

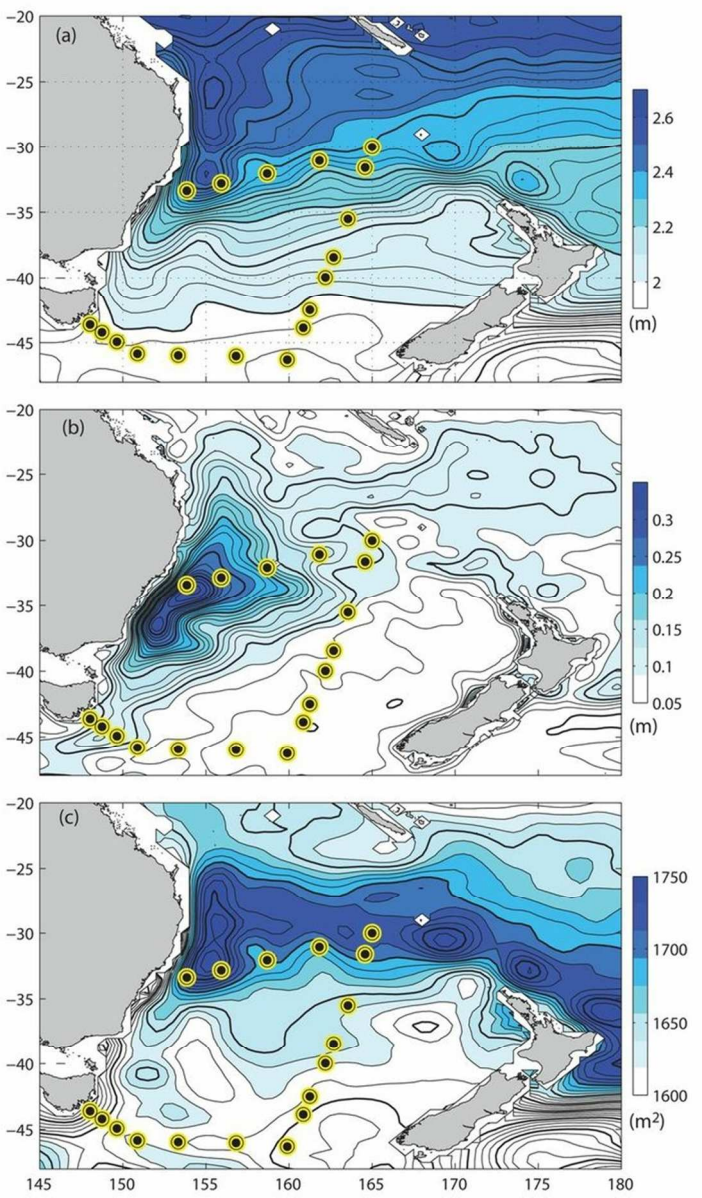

246x423mm (72 x 72 DPI)

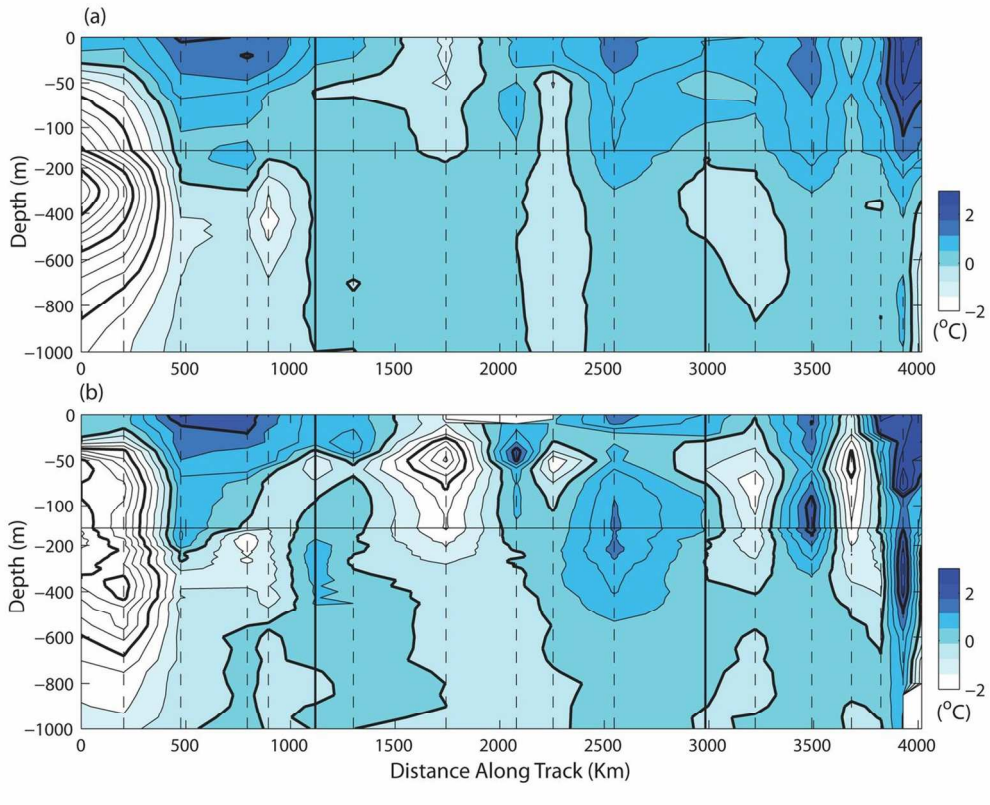

518x423mm (72 x 72 DPI)

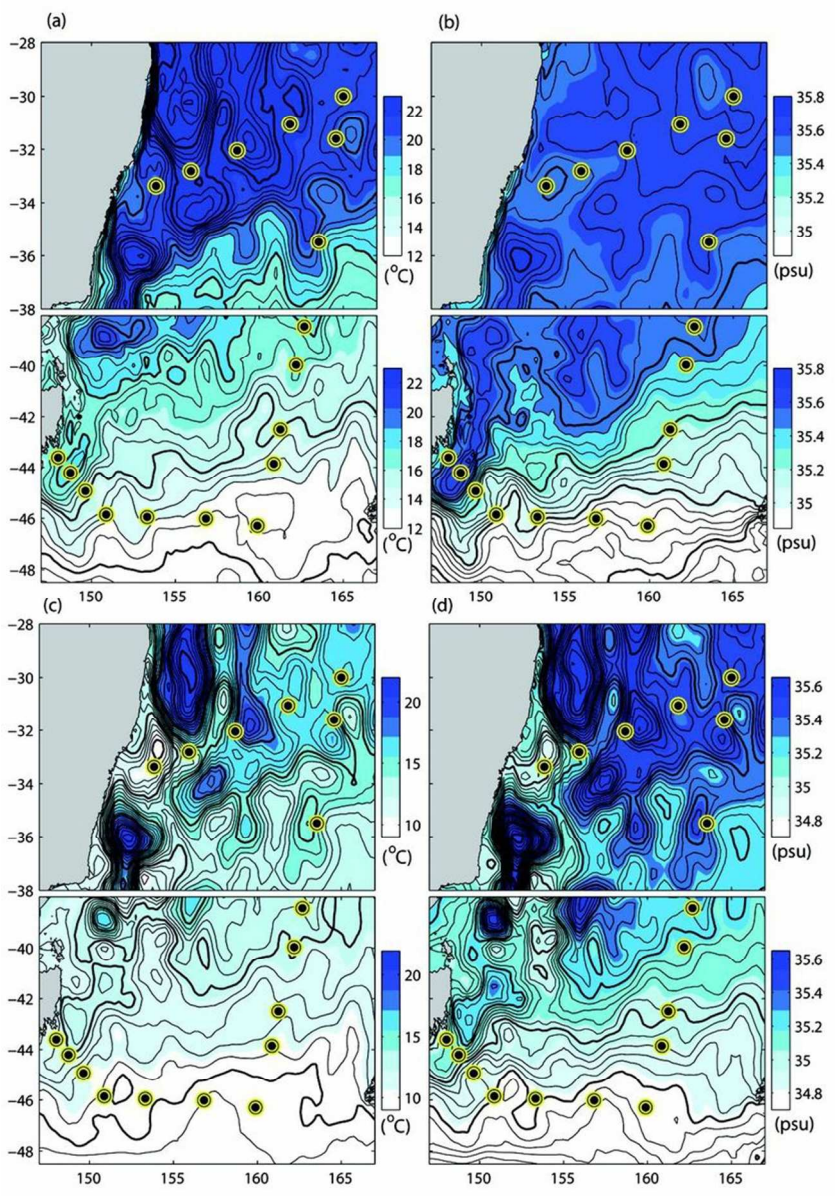

293x423mm (72 x 72 DPI)

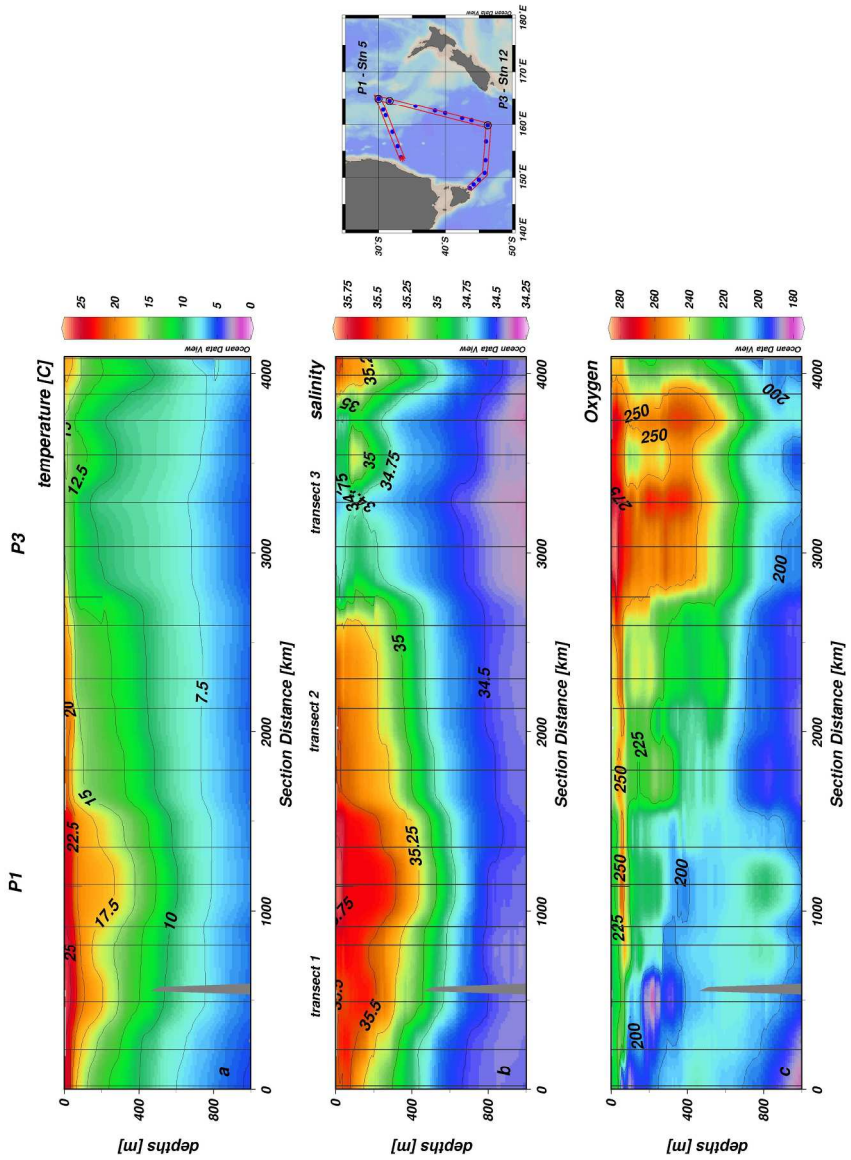

206x278mm (300 x 300 DPI)

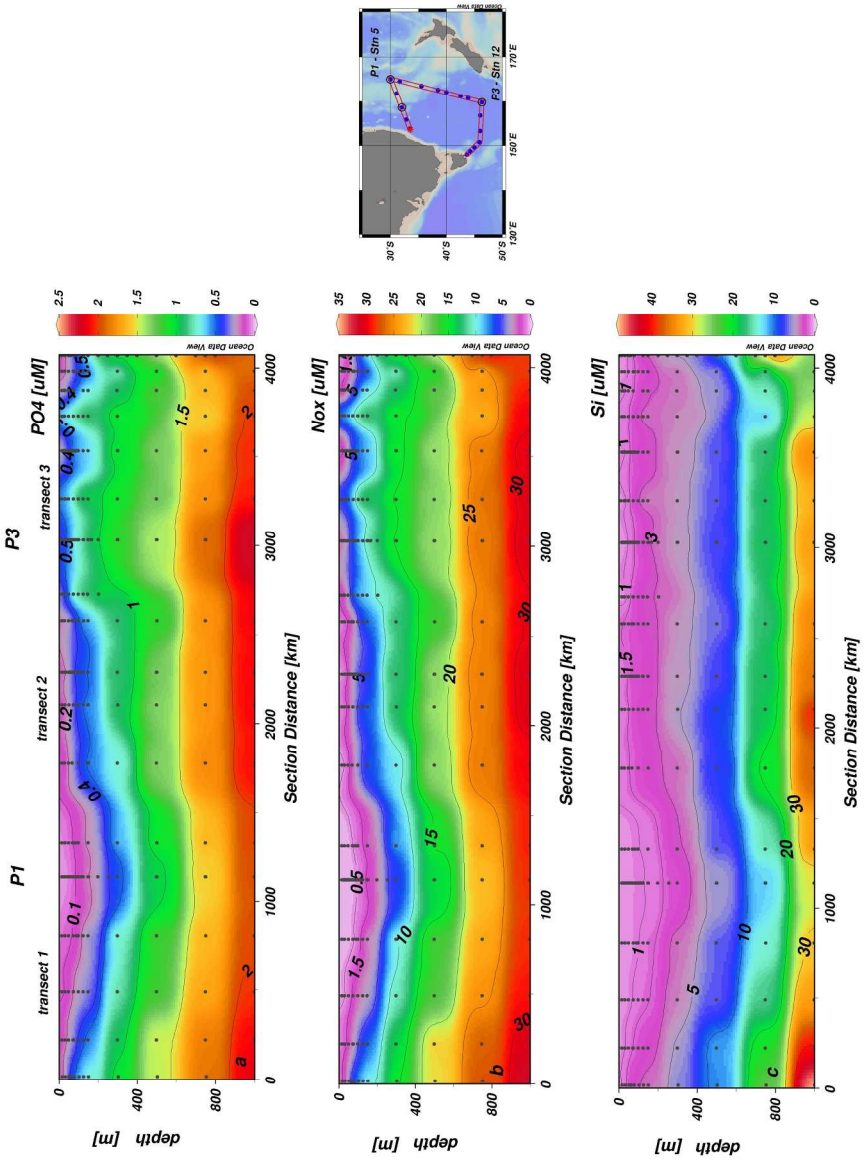

196x259mm (300 x 300 DPI)

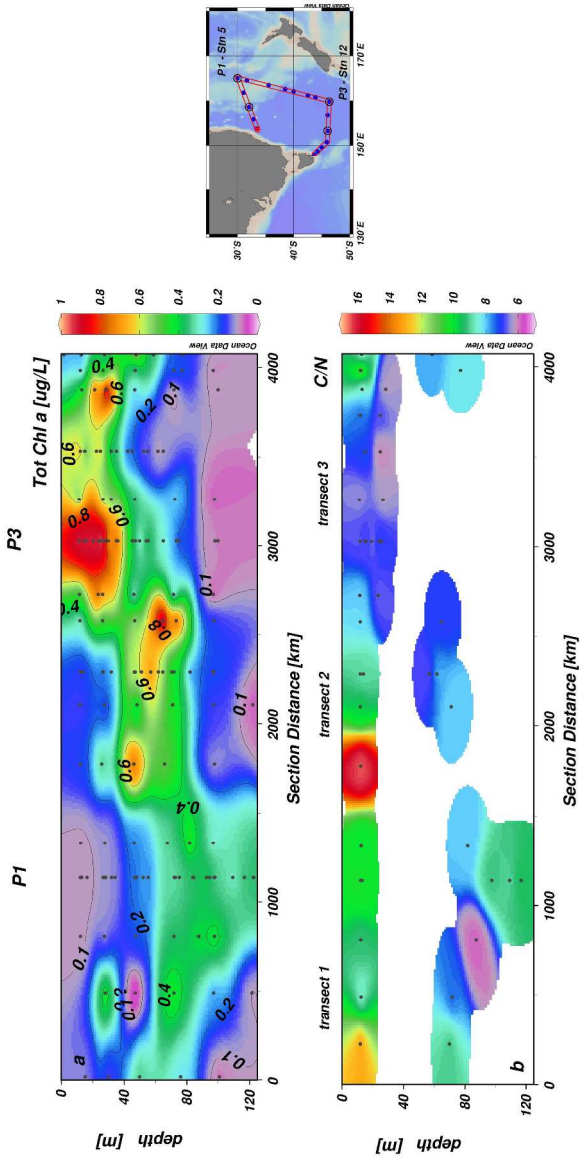

196x377mm (300 x 300 DPI)

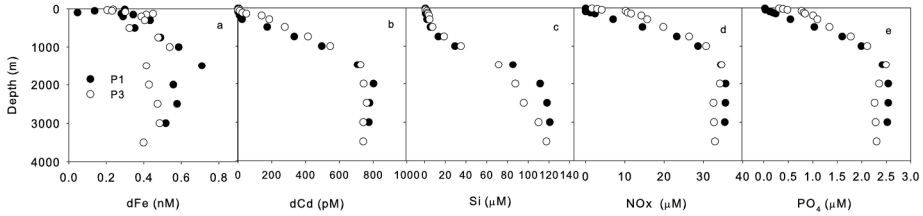

209x147mm (300 x 300 DPI)

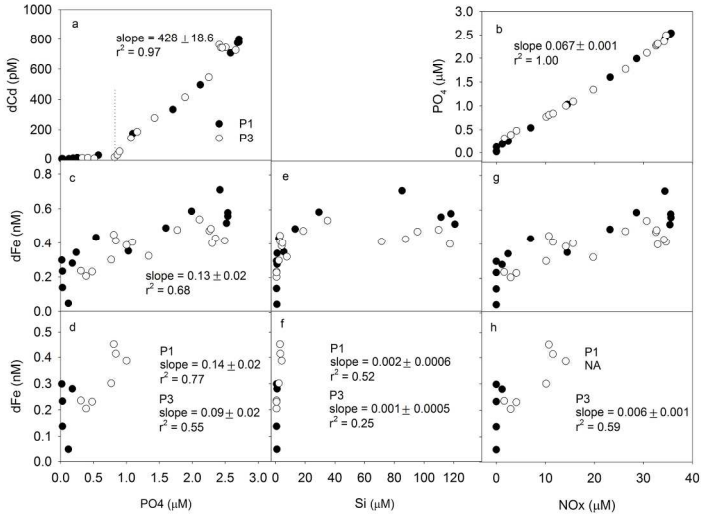

209x147mm (300 x 300 DPI)

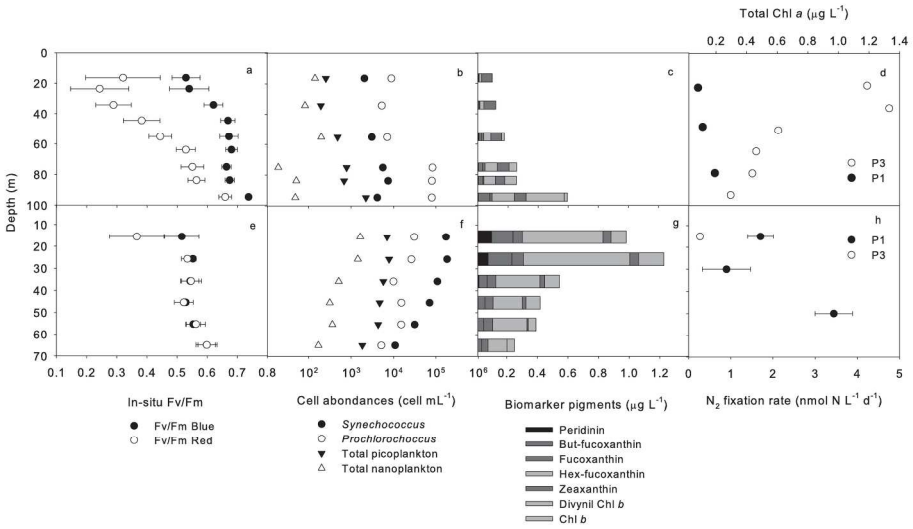

209x147mm (300 x 300 DPI)

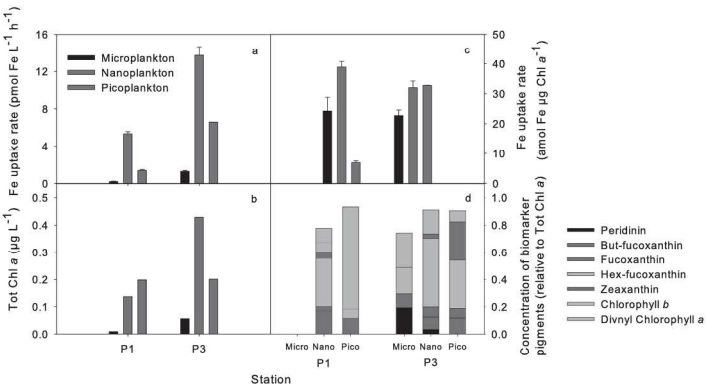

209x148mm (300 x 300 DPI)

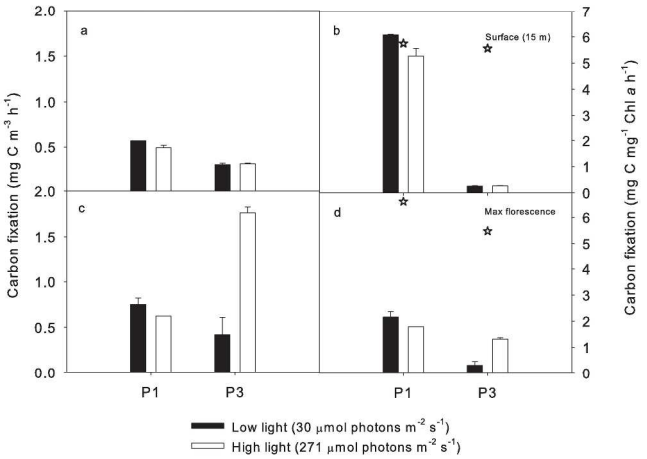

296x420mm (300 x 300 DPI)